Study of vibrational kinetics of CO 2 and CO in CO 2 –O 2 plasmas under non-equilibrium conditions

C Fromentin, T Silva, T Dias, A Morillo-Candas, O Biondo, O Guaitella, V Guerra

Plasma Sources Science and Technology

PAPER • OPEN ACCESS

Study of vibrational kinetics of CO_2 and CO in CO_2–O_2 plasmas under non-equilibrium conditions

To cite this article: C Fromentin *et al* 2023 *Plasma Sources Sci. Technol.* **32** 024001

OPEN ACCESS
IOP Publishing
Plasma Sources Science and Technology
Plasma Sources Sci. Technol. **32** (2023) 024001 (26pp)
https://doi.org/10.1088/1361-6595/acb665

Study of vibrational kinetics of CO_2 and CO in CO_2–O_2 plasmas under non-equilibrium conditions

C Fromentin[1], T Silva[1], T C Dias[1], A S Morillo-Candas[2,4], O Biondo[3], O Guaitella[2] and V Guerra[1,*]

[1] Instituto de Plasmas e Fusão Nuclear, Instituto Superior Técnico, Universidade de Lisboa, Lisbon, Portugal
[2] Laboratoire de Physique des Plasmas (UMR 7648), CNRS, University Paris Saclay, Sorbonne Université, École Polytechnique, Palaiseau, France
[3] Plasma Lab for Applications in Sustainability and Medicine—ANTwerp, Antwerp, Belgium

E-mail: vguerra@tecnico.ulisboa.pt

Received 14 October 2022, revised 27 December 2022
Accepted for publication 26 January 2023
Published 9 February 2023

Abstract

This work explores the effect of O_2 addition on CO_2 dissociation and on the vibrational kinetics of CO_2 and CO under various non-equilibrium plasma conditions. A self-consistent model, previously validated for pure CO_2 discharges, is further extended by adding the vibrational kinetics of CO, including electron impact excitation and de-excitation (e-V), vibration-to-translation relaxation (V-T) and vibration-to-vibration energy exchange (V-V) processes. The vibrational kinetics considered include levels up to $v = 10$ for CO and up to $v_1 = 2$ and $v_2 = v_3 = 5$, respectively for the symmetric stretch, bending and asymmetric stretch modes of CO_2, and accounts for e-V, V-T in collisions between CO, CO_2 and O_2 molecules and O atoms and V-V processes involving all possible transfers involving CO_2 and CO molecules. The kinetic scheme is validated by comparing the model predictions with recent experimental data measured in a DC glow discharge ignited in pure CO_2 and CO_2–O_2, operating at pressures in the range 0.4–5 Torr (53.33–666.66 Pa). The experimental results show a lower vibrational temperature of the different modes of CO_2 and a decreased dissociation fraction of CO_2 when O_2 is added to the plasma but an increase of the vibrational temperature of CO. On the one hand, the simulations suggest that the former effect is the result of the stronger V-T energy-transfer collisions with O atoms which leads to an increase of the relaxation of the CO_2 vibrational modes. On the other hand, two main mechanisms contribute to the lower CO_2 dissociation fraction with increased O_2 content in the mixture: the back reaction, $CO(a^3\Pi_r) + O_2 \rightarrow CO_2 + O$ and the recombinative detachment $O^- + CO \rightarrow e + CO_2$.

[4] Current affiliation: Paul Scherrer Institut, CH-5232 Villigen PSI, Switzerland.
[*] Author to whom any correspondence should be addressed.

Supplementary material for this article is available online

Keywords: vibrational kinetics, DC glow discharge, reaction mechanism, CO_2 conversion, low-temperature plasma, model validation

(Some figures may appear in colour only in the online journal)

1. Introduction

The growing concentration of greenhouse gases in the atmosphere coming from anthropogenic activities [1], and the resulting climate change are a great concern of our century. As CO_2 has the most important contribution to global warming [2], it is necessary to focus on reducing its concentration in the atmosphere via carbon capture and utilization, for instance, for chemical synthesis and fuel production [3], ideally using electricity from renewable energy sources, and CO_2 from industrial emissions as a feedstock. However, CO_2 is, thermodynamically, a very stable molecule so the conversion of CO_2 is limited by the initial dissociation step ($CO_2 \rightarrow CO + O$). The conventional heating of the gas can be used in principle to split CO_2 molecules. However, the high energy cost of this method, among other limitations, make technologies like non-thermal plasmas (NTP) very attractive for CO_2 conversion [4–10]. NTPs are characterized by non-equilibrium conditions, where high energy electrons and cold heavy species concur, which are ideal for the breaking of chemical bonds while they can be operated at room temperature and atmospheric pressure.

CO_2-containing discharges are intensively studied nowadays, both in terms of experimental work and modelling [5, 9–24] to bring new insights into the kinetics of CO_2 dissociation by different pathways. The CO_2 dissociation by direct electron impact requires at least 7 eV and produces O in an electronically excited state and CO [25]. However, by taking advantage of non-equilibrium plasma processes, only 5.5 eV may be required to obtain the products in the ground state via stepwise vibrational excitation of CO_2 by anharmonic vibration-to-vibration energy exchange (V-V) up pumping to the dissociation limit [26]. Having said that, the vibrational state of CO_2 is also affected by the interplay between all the vibrational modes, through vibrational-translational transitions, intermode vibrational-vibrational exchanges, intermolecular vibrational-vibrational exchanges (like CO_2–CO V-V) and state-specific dissociation/recombination reactions [27].

Following the measurements of Klarenaar *et al* in a pulsed CO_2 glow discharge [16], Silva *et al* studied the complex kinetics of the relaxation of vibrationally excited CO_2 levels during the afterglow validating a set of vibration-to-translation relaxation (V-T) and V-V energy transfer processes and the corresponding rate coefficients [17]. Moreover, in [18] the investigation focuses as well on the active discharge, by extending the model with the inclusion of electron impact processes for vibrational excitation and de-excitation (e-V) [17–19]. In parallel, Silva *et al* established a reaction mechanism (i.e. a set of reactions and rate coefficients validated against benchmark experiments) for 'vibrationally cold CO_2 plasmas', considering the CO_2 dissociation products, validated by comparing simulation results with experimental data measured in continuous CO_2 glow discharges where dissociation cannot be neglected [14]. Other modelling research works focused on the electron-neutral scattering cross sections for CO_2 [28] and CO [29], the electron-impact dissociation cross sections of CO_2 [15], the dynamics of gas heating in the afterglow of pulsed CO_2 and CO_2–N_2 glow discharges at low pressure further validating the V-V and V-T mechanisms and rate coefficients [21], the CO_2 dissociation under Martian environment for oxygen production [11, 30, 31] and the role of electronically excited metastable states in CO_2 dissociation and recombination [32]. More information about these works can be found in [22] where recent advances in non-equilibrium CO_2 plasma kinetics are reviewed.

Herein we extend the study of the coupled electron, vibrational and chemical kinetics developed in [11, 14, 17–19] with the addition and validation of the CO vibrational kinetics, by including 10 vibrational levels of CO, and an accurate description of the vibrational kinetics involving the dissociation products, namely CO, O_2, O as was initiated in [11]. This constitutes a major improvement regarding our previous simulations for CO_2 plasmas and is relevant as CO is a product of the CO_2 dissociation and therefore always present in CO_2 gas discharges. In parallel, we address the study of CO_2–O_2 mixtures. Indeed, investigating the influence of O_2 on the CO_2 dissociation is pertinent as O_2 is an impurity often present in industrial emissions [33]. In addition, O_2 is also one of the main by-products of the dissociation of CO_2, formed from the recombination of O atoms. The admixture of O_2 has a detrimental impact on CO_2 decomposition, as shown experimentally in [12], as it leads to a decrease of the CO_2 dissociation fraction via the enhancement of the reverse reaction ($CO(a^3\prod_r) + O_2 \rightarrow CO_2 + O$), producing back CO_2 from electronically excited CO, $CO(a^3\prod_r)$, in collisions with O_2 [13]. Besides, the presence of oxygen in the discharge influences greatly the vibrational kinetics of CO_2 and CO mostly via the quenching with O atoms [34]. Finally, by varying the O_2 content in CO_2–O_2 mixtures we enlarge the parameter space and can have a thorough validation of the model and gain a deeper understanding of the kinetics of CO_2 plasmas.

To establish a reaction mechanism for vibrationally excited CO_2 and CO_2–O_2 plasmas a DC glow discharge (plasma sustained by high voltages inside a pair of electrodes) is used as it generates a stable (axially) homogeneous plasma (in the positive column) and is accessible to different diagnostics and therefore optimal for model validation. The CO_2 and CO densities and its vibrational kinetics are diagnosed by FTIR

spectroscopy, and actinometry is used to determine the O atom density and O loss frequency.

The paper is structured as follows. Section 2 provides information about the experimental setup and the diagnostics used. In section 3 the model is described, and the kinetic scheme used to study the CO_2 discharge is specified. Moreover, in this section we also detail some rate coefficients for electron impact reactions, vibration-translation and vibration-vibration exchanges involving CO_2 and CO. The comparison between the experiments and the simulations is presented and discussed in section 4 to gain further insight into the underlying kinetics. Finally, section 5 summarizes the main findings of this work.

2. Experiment

The plasma discharge setup used to obtain the data described in this work consists of a continuous DC glow discharge ignited in a cylindrical Pyrex tube of 1 cm radius in a pure CO_2 or a CO_2–O_2 gas mixture. Two different reactor lengths were used, 67 cm for actinometry and 23 cm for *in situ* Fourier Transform Infrared (FTIR) spectroscopy experiments with the electrodes positioned 53 or 17 cm apart, respectively, depending on the tube length and opposite to the gas in- and outlet. Two discharge currents were used, 20 and 40 mA, and the pressure varied between 0.4 and 5 Torr, using a scroll pump (Edwards XDS-35), and a pressure gauge (Pfeiffer CMR263) with feedback to an automated pressure regulating valve (Pfeiffer EVR116) and controller (Pfeiffer RVC300). The reactor is connected in series with a 40 kΩ resistor to a DC power supply. The gas flows are controlled using mass flow controllers (Bronkhorst F-201CV). A total gas flow of 7.4 sccm is used as the reference condition in the present experiments as previously employed in [11, 16, 20, 35, 36]. The experimental set-up and measurement techniques (actinometry and FTIR spectroscopy) are presented and described in detail in [16, 35].

The CO_2 and CO vibrational and rotational temperatures and dissociation fraction are obtained by *in situ* FTIR spectroscopy using a Bruker V70 FTIR spectrometer with 0.2 cm^{-1} spectral resolution. These quantities are obtained as an outcome of the fitting of the measured IR spectra containing several lines of CO and CO_2 vibrational transitions, as described by Klarenaar *et al* in [16, 36], in a 23 cm long reactor. The rotational temperature (T_{rot}) can be assumed to be in equilibrium with the gas temperature (T_g) [35] and is used as an input parameter for our model. The quantities obtained by FTIR spectroscopy are approximately an average over the radius of the reactor since the FTIR beam fills most of the discharge tube and it is assumed that the rotational and vibrational temperatures are uniform along the length of the reactor. The sensitivity of the fitted transmittance to the different temperatures can give an indication of their error, which was estimated to be 30 K and 27 K for T_{rot} and $T_{1,2}$ respectively, 67 K for T_3 and 357 K for T_{CO} at 5 Torr, 50 mA and in pure CO_2 [16]. This estimation of the accuracy of the fit was done by Klarenaar *et al* in [16] and only for one condition with the best signal to noise ratio in the range explored, therefore, we can assume that these values correspond to a minimum error.

The average electric field in the plasma bulk is estimated by measuring the voltage drop in the positive column, considered homogeneous, between two tungsten probes, at the floating potential, pointing radially inside the reactor.

The experimental characterization of the discharge comprises the determination of O atom densities and O loss frequencies by actinometry measured in a 67 cm length tube [35]. The measured loss frequencies, ν_{loss}, can be the result of both surface loss processes and/or gas phase reactions [35]:

$$\nu_{loss} = \frac{v_{th} \cdot \gamma_O}{2 \cdot R} + L_{gp}, \tag{1}$$

where L_{gp} represents the contribution of the gas phase losses, γ_O is the O atom surface loss probability, v_{th} is the thermal velocity of the O atoms and R is the radius of the discharge tube. In the present conditions the contribution of gas phase losses can be discarded [35] and expression (1) becomes:

$$\gamma_O = \frac{2 \cdot R \cdot \nu_{loss}}{v_{th}}, \tag{2}$$

where

$$v_{th} = \sqrt{\frac{8 \cdot k_B \cdot T_g}{\pi \cdot m}}, \tag{3}$$

k_B is the Boltzmann constant, m the mass and T_g the gas temperature. The error on the loss frequency (from which is calculated the recombination probability, cf equation (2)), related to the reproducibility of the experiment, is of the order of 15%. The O densities measured using actinometry rely on many rate coefficients particularly on the choice of electron impact excitation cross sections and are given with a minimum error of 30% [35].

In this work we will discuss three data sets. In the first one we have varied the CO_2–O_2 gas mixture (Air Liquide Alphagaz 1 for CO_2 a Alphagaz 2 for O_2). The FTIR experiments were done in the 23 cm reactor and the error bars on T_{CO} being so large when O_2 is added to the mixture we only provide the experimental data for the pure CO_2 case. The large uncertainty on the CO temperatures measured by FTIR is due to the low signal to noise ratio for the CO band particularly at low pressures and currents and high O_2 content, corresponding respectively to low particle density and low CO concentrations. The relative fitting error on the dissociation fraction was calculated and is lower than 2% for all the conditions measured. The O atom surface loss probabilities, γ_O, used in this work for the simulations of the CO_2–O_2 mixture can be found in table 1. They were obtained from loss frequency measurements as detailed in [35], in the 67 cm reactor. In the same reactor the atomic oxygen fraction was determined using actinometry and is defined as the number of oxygen atoms divided by the gas density N. It is important to note that the loss frequencies were obtained for a wall temperature T_{wall} of the Pyrex tube of 25 °C whereas the temperatures obtained by FTIR spectroscopy were obtained for $T_{wall} = 50$ °C. The effect was verified to be around 30 K for T_3 and 20 K for $T_{1,2}$

and therefore considered negligible as it lays within the experimental error.

The CO_2 dissociation fraction obtained in the short tube (23 cm) can be extrapolated for the longer tube (67 cm), where the O atom measurements were taken. This was possible by measuring the dissociation fraction and vibrational and rotational temperatures as a function of the residence time since downstream measurements using both long and short tubes confirmed that the CO_2 dissociation fraction is the same in both reactors, for a given residence time, in pure CO_2 [35]. Moreover, the temperatures for the same pressure and current are assumed to be the same in both reactors due to the fast timescales of temperature evolution in comparison with the residence times in the experimental conditions.

We recall a second dataset, containing the vibrational and rotational temperatures of CO_2 and CO, the reduced electric field, *E*/*N*, the fractions of O an CO and surface O loss probabilities, γ_O, for the pure CO_2 case since it contains data for an extended pressure range and can be found in [35]. Finally, another data set presented in [34] for pure CO_2 is also analysed in section 4.4. It consists of a Pyrex tube (23 cm length) but covered with micro-structured silica fibres enhancing the O recombination at the walls. The vibrational and rotational temperatures of CO_2 and CO were measured with *in situ* FTIR spectroscopy and the surface O loss probabilities, γ_O, are taken from [35].

3. Model

3.1. General formulation

The self-consistent global model used in this work couples the homogeneous two-terms approximation Boltzmann equation for the electrons to a set of zero-dimensional (spatially averaged) rate balance equations describing the creation and destruction of the neutral and charged heavy species considered. The simulations are performed with the Lisbon Kinetics (LoKI) [37, 38] numerical code, composed of two modules:

LoKI-B: solves the time and space independent electron Boltzmann equation within the two-terms approximation, for non-magnetised non-equilibrium low-temperature plasmas (LTPs) excited by DC/HF electric fields for different gases or gas mixtures and provides the electron energy distribution function (EEDF), electron transport parameters and electron impact rate coefficients;

LoKI-C: solves a system of zero-dimensional time-dependent rate balance equations for the heavy species assuming a fixed pressure, until steady state is reached.

The complete description of the workflow of LoKI can be found in [14]. The electron, chemical and vibrational kinetics are coupled into a self-consistent scheme for which the reduced electric field, *E*/*N*, corresponds to steady-state conditions where the total rate of production of electrons in ionization events must compensate exactly their total loss rate due to ambipolar diffusion to the wall and electron-ion recombination, while satisfying the quasi-neutrality condition.

The diffusion scheme adopted to describe the charged-particles losses is the ambipolar diffusion to the reactor walls. For the heavy species, including the vibrationally excited species, we use the Chantry model [39] to obtain the loss rate of a particular species interacting with the wall due to the combined effect of transport (with a diffusion coefficient) and the reaction at the wall (with a certain wall recombination/deactivation probability γ) [20, 40]. The renewal of the gas in the reactor influences the densities of the species in the plasma and was thus included in the model. The rate coefficient for the inlet and outlet flow of species is calculated assuming conservation of atoms in the gas/plasma mixture as described in [14]: new CO_2/O_2 particles enter the reactor while the species produced in the plasma exit at the outlet.

The input parameters of the model are the gas pressure (*P*), discharge current (*I*) and the initial gas mixture and corresponding gas flows controlled during the experiment (see section 2), as well as the dimensions of the experimental reactor. The loss probability of O atoms at the wall, γ_O, is also included as input parameter and deduced from the experimental determination of O-atom loss frequencies (see table 1 for the CO_2–O_2 mixture and [35] for pure CO_2). Additionally, in the present simulations the gas temperature is also given as an input parameter since its value is available from experiment and our purpose is not to focus on the gas heating mechanisms but rather on the plasma chemistry. However, the gas thermal balance equation can be incorporated in the current formulation of the model as already done in [21, 41, 42] for the study of gas heating mechanisms. The average electron density was calculated based on the discharge current and the electron drift velocity obtained from the Boltzmann equation solution.

Using as input the parameters that are controlled/measured during a glow discharge experiment and listed above, one is able to obtain: the reduced electric field, *E*/*N*, the electron density, the EEDF (obtained in a CO_2/CO/O_2/O mixture), all the swarm parameters (electron temperature, mobility, drift velocity, etc), collision rate coefficients and power transfer in each electron impact collision process), the various heavy-particle reaction rates and species densities and, thus, the CO_2 dissociation fraction.

3.2. Kinetic scheme

A kinetic description of both electrons and heavy species is needed to accurately describe the plasma under study. For the electron kinetics we use a complete and consistent set of cross sections from the IST-Lisbon database retrieved in June 2020, available on the open-access website LXCat [43, 44], and described in [28] (for CO_2) [45, 46], (for O and O_2) and [29] (for CO). It is worth noting that in the Boltzmann solver the superelastic electronic collisions with the different rotational, vibrational and electronic states of these molecules are taken into account.

The cross section set used for CO_2 [28] and based on the Phelps database [47] contains two electronic excitation cross sections, with thresholds at 7 eV and 10.5 eV. These excitation levels most likely represent dissociative channels and probably contain more than just dissociation [28]. Note that the Polak and Slovetsky's total cross sections used for the electron-impact dissociation of CO_2 [25] are not part of the

Table 1. O atom surface loss probabilities, γ_O, for different CO_2–O_2 mixtures, pressures, and discharge currents, calculated from the experimental loss frequency measurements. *extrapolated values.

CO_2 initial fraction		0.25	0.5	0.75	1
Pressure (Torr)	Current (mA)	O loss probability			
1	20	0.000454458	0.000386444	0.000282906	0.000212388
2	20	0.000531294	0.000445574	0.000290678	0.000201258
5	20	0.000697701*	0.000662973	0.000427483	0.000353317
1	40	0.000739642	0.000616286	0.000468980	0.000284431
2	40	0.000917035	0.000645062	0.000524091	0.000357731
5	40	0.001163260*	0.000925654	0.000650424	0.000466082

Table 2. Species considered in the chemistry module, LoKI-C.

$CO_2(X^1\Sigma^+{}_g,v^*)$	$CO(X^1\Sigma^+,v^*)$	$O_2(X^3\Sigma_g{}^-)$	$O(^3P)$	$C(^3P)$	O_3 (X^1A_1)
	$CO(a^3\Pi_r)$	$O_2(a^1\Delta_g)$	$O(^1D)$		$O_3{}^*$
		$O_2(b^1\Sigma_g{}^+)$			
$CO_2{}^+$	CO^+	$O_2{}^+$	O^+		
			O^-		

complete and consistent CO_2 cross section set and, accordingly, are not used to obtain the EEDF, but are integrated with the calculated EEDF to obtain the corresponding rate coefficient as suggested in [15]. Concerning the Polak and Slovetsky's total cross sections for electron-impact dissociation of CO_2, Morillo-Candas *et al* [15] validated the electron impact CO_2 dissociation cross sections, in the range of reduced electric fields 40–110 Td using two complementary methods: through the comparison of the measured rate coefficients in a large range of reduced electric fields with those derived from cross sections, available in literature; and through the comparison of the experimental time evolution of the dissociation fraction with the simulations of a 0D model and thus recommend the use of these cross sections for the calculation of the CO_2 electron impact dissociation rate under those discharge conditions.

The complex plasma chemistry used in this work is based on previous publications dealing with CO_2 vibrations [17–19], kinetic mechanisms in O_2 plasmas [48], and plasma chemistry in vibrationally cold CO_2 [14] and includes the following species (table 2): ground-state and electronically excited CO, CO_2 and O_2 molecules $CO(X^1\Sigma^+)$, $CO(a^3\Pi_r)$, $CO_2(X^1\Sigma^+{}_g)$, $O_2(X^3\Sigma_g{}^-)$, $O_2(a^1\Delta_g)$, $O_2(b^1\Sigma_g{}^+)$; ground-state and electronically excited oxygen atoms, $O(^3P)$, $O(^1D)$, ground-state carbon $C(^3P)$, ground-state ozone and vibrationally excited ozone, O_3, $O_3{}^*$; and positive and negative ions, O^+, O_2^+, O^-, CO_2^+, CO^+. For $O_3{}^*$ we consider a single effective vibrationally excited state [49]. Note that tables summarizing the processes used in our chemistry set and the corresponding rate coefficients are given in [14, 48], for CO_2 and O_2 respectively, and therefore are not reproduced in the present work. For the kinetics of oxygen, the set proposed in [48] is adopted without modifications except for the exclusion of vibrational states in the heavy species chemistry and the use of the measured loss frequency of the ground state of atomic oxygen. We further use the chemistry set proposed by Silva *et al* in [14] for vibrationally-cold low-pressure CO_2 plasmas, to which we added the three-body reactions:

$$O + CO + M \rightarrow CO_2 + M,\ M = CO_2, CO, O_2,$$

with the rate coefficients taken from [50].

In the present conditions of pressures and temperatures, the three-body reactions play a negligible role [14] and the dominant 'back reaction' should be a 2-body mechanism [51]. However, three-body processes could be relevant to properly describe the recombination of CO_2 at high pressure conditions, of interest for plasma reforming for instance; therefore, we include them in the current formulation of the model for completeness.

3.3. Vibrational kinetics

The present work studies the state-to-state kinetics of the first 72 low-lying levels of CO_2 plasma during the active discharge, corresponding to CO_2 ($\nu_1{}^{max} = 2$, $\nu_2{}^{max} = \nu_3{}^{max} = 5$), where ν_1, ν_2 and ν_3 are quantum numbers of the symmetric stretching, bending, and asymmetric stretching vibrational modes, respectively, with energies up to about 2 eV and the first 10 levels of CO with energy up to about 2.5 eV [17] and a normalized population of around 10^{-6} for $v = 10$. Describing only the low-lying vibrational levels is enough to describe accurately the most important electron energy exchanges and modifications of the EEDF due to inelastic and superelastic collisions with the vibrationally excited states. Moreover, due to the low excitation regime found in glow discharges the vibrational populations of highly excited states are not expected to influence the plasma chemistry by activating endothermic reactions like the CO_2 dissociation [14, 34, 36]. Finally, the model developed by Silva *et al* [17–19] and containing the same 72 levels for CO_2, was thoroughly validated in similar conditions

as in this study although only for pure CO_2 and low dissociation, from the good comparison obtained between the calculated time-dependent populations of vibrationally excited states with measurements obtained by time-resolved *in situ* FTIR spectroscopy in a pulsed DC glow discharge. While the vibrational kinetics of CO_2 and CO are included in the rate balance equations, the vibrational kinetics of O_2 are only considered in the Boltzmann solver to obtain the EEDF. The first four vibrational levels are considered for the EEDF calculation, assuming a Boltzmann distribution at the gas temperature. The inclusion of vibrationally excited O_2 molecules in the chemistry module does not influence the simulation results [48] (densities, *E*/*N* etc) for our conditions but significantly increases the computation time. For the conditions studied here, the vibrational distribution function of O_2 shows a steep decrease already at low vibrational levels (relative population of the $v = 2$ level $\sim 10^{-6}$).

The density of the different vibrationally excited levels is governed by the rate of creation and loss by electron impact, vibrational-translational and vibrational-vibrational exchanges and chemical reactions and processes like dissociation or ionization [18]. Due to the lack of data, the dissociation cross sections via electron impact from vibrationally excited states are considered with a threshold shift, while keeping the same amplitude as for dissociation from the ground-state [11]. The same procedure is used for ionization from vibrationally excited CO and CO_2 molecules (and attachment for CO_2). We do not consider dissociation through the pure vibrational path, but only stepwise dissociation by electron impact on vibrationally excited CO_2. The validity of this assumption is shown and discussed in [14]. However, under extreme conditions, such as those encountered on Mars atmospheric entry, one should consider higher vibrational levels and CO_2 dissociation via the pure vibrational process. Two models are commonly used in the literature: the ladder-climbing model assuming dissociation only from the last vibrational level and that of Treanor and Marrone [52] allowing for dissociation from any vibrational state [53]. It was suggested that the ladder climbing model based on the asymmetric vibrational mode significantly underpredicts the dissociation rate and the generalized Marrone-Treanor model (including the different modes up to the dissociation limit) was recommended as it can predict correctly the state-resolved dissociation rate coefficients in CO_2 [54].

Following the approach in [17–19], the CO_2 vibrational levels are described by four quantum numbers using the notation $CO_2(v_1v_2{}^{l2}v_3f)$, also known as Herzberg's form [55]. In the present work the CO_2 vibrational levels under Fermi resonance are considered as one single effective level. The Fermi resonance refers to an accidental energy degeneracy between certain vibrational modes. In the case of CO_2, the modes ν_1 and $2 \cdot \nu_2$ have very close vibrational energies, resulting in a coupling between the $CO_2(v_1v_2{}^{l2}v_3)$ and $CO_2((v_1\text{-}1)(v_2+2)^{l2}v_3)$ levels to form new states that are assumed to be in local equilibrium. All the vibrational levels coupled together have the same orbital quantum number l_2 (projection of the angular momentum of bending vibrations) since those with different l_2 cannot perturb each other. The ranking number f is always equal to $\nu_1 + 1$ and indicates how many individual levels are accounted for in the effective level [17].

Table 3. Spectroscopic constants for the calculation of energy levels using (4), obtained from [56].

Constant	cm^{-1}
$\omega 1$	1335.879
$\omega 2$	667.2044
$\omega 3$	2361.647
$\chi 11$	−2.99262
$\chi 12$	−5.27638
$\chi 13$	−19.14044
χll	−1.01428
$\chi 22$	1.583
$\chi 23$	−12.54184
$\chi 33$	−12.50330
$\gamma 111$	0.02422
$\gamma 112$	0.00816
$\gamma 113$	−0.07736
$\gamma 1ll$	0.06316
$\gamma 122$	−0.05166
$\gamma 123$	0.09561
$\gamma 133$	0.06142
$\gamma 2ll$	0.0072
$\gamma 222$	−0.00471
$\gamma 3ll$	0.02587
$\gamma 223$	−0.02052
$\gamma 233$	0.01834
$\gamma 333$	0.00631

The energies of the individual levels are calculated according to the anharmonic oscillator approximation and are based on [56] using the spectroscopic constants from table 3.

$$\begin{aligned}\frac{E(v_1,v_2,l_2,v_3)}{h\cdot c} &= w_1\cdot v_1 + w_2\cdot v_2 + w_3\cdot v_3 + x_{11}\cdot v_1^2 \\ &\quad + x_{22}\cdot v_2^2 + x_{ll}\cdot l_2 + x_{33}\cdot v_3^2 \\ &\quad + x_{12}\cdot v_1\cdot v_2 + x_{13}\cdot v_1\cdot v_3 + x_{23}\cdot v_2\cdot v_3 \\ &\quad + y_{111}\cdot v_1^3 + y_{112}\cdot v_1^2\cdot v_2 + y_{113}\cdot v_1^2\cdot v_3 \\ &\quad + y_{122}\cdot v_1\cdot v_2^2 + y_{123}\cdot v_1\cdot v_2\cdot v_3 \\ &\quad + y_{133}\cdot v_1\cdot v_3^2 + y_{222}\cdot v_2^3 + y_{223}\cdot v_2^2\cdot v_3 \\ &\quad + y_{233}\cdot v_2\cdot v_3^2 + y_{333}\cdot v_3^3 + y_{1ll}\cdot v_1\cdot l_2^2 \\ &\quad + y_{2ll}\cdot v_2\cdot l_2^2 + y_{3ll}\cdot v_3\cdot l_2^2 \end{aligned} \quad (4)$$

With h the Planck constant and c the speed of light. Such calculation should be solved also for the ground state $CO_2(00^00)1)$ as it results in an energy value $\neq 0$ eV. The resulting value is to be subtracted to all the level energies in order to have the ground state at 0 eV and all the vibrational levels normalized to it. The calculated values were compared with experimental spectroscopic data available in [57] and show a good agreement.

The vibrational energy of the effective level is determined through the average of the vibrational energies of all the individual levels in the effective level and we assume that the average energy of unperturbed levels is the same as the average

energy of the levels perturbed by the Fermi resonance coupling. The statistical weight is determined through the sum of the statistical weights of the individual states.

The CO vibrational energy levels can be calculated by the formula [58]:

$$\frac{E_{co}}{hc} = \omega_{e.}\,(v+0.5) - \omega_e \cdot x_e \cdot (v+0.5)^2 \qquad (5)$$

where v is the vibrational quantum number, ω_e is the vibrational frequency, x_e is the non-dimensional anharmonicity, h the Plank constant and c the speed of light. We use the values $\omega_e = 2169.81\ \mathrm{cm}^{-1}$ and $\omega_e \cdot x_e = 13.29\ \mathrm{cm}^{-1}$, obtained from the NIST Chemistry WebBook [59]. Only the first 10 vibrational levels of CO, up to the energy of 2.51 eV, are included in the model as it is already higher than the energy of the highest CO_2 vibrational level included. Moreover, they are enough to calculate accurately the vibrational temperatures of CO and CO_2 in the present conditions (cf section 4), as the relative population of $v = 10$ is always smaller than 5×10^{-6}.

3.3.1. e-V. The cross sections for the e-V reactions included in our model are obtained from a direct deconvolution of the available lumped cross sections [28] according to the statistical weights of the various levels (bending and symmetric stretch modes), as reported by Grofulović *et al* [18]. For the transitions from the ground state to the higher vibrationally excited levels that are not included in any of the cross sections from the data set [28], namely for the asymmetric mode, we have used the semiempirical Fridman approximation [26]. The rate coefficient k_{ij} of the excitation from $CO_2(v_1v_2{}^{l2}i1)$ to $CO_2(v_1v_2{}^{l2}j1)$ is given by:

$$k_{ij} = \frac{\exp[-\alpha_f \times (j-i-1)]}{1+\beta \times i} k_{01}, \qquad (6)$$

with k_{01} the rate coefficient for the excitation from the ground state to the first excited state corresponding to the process $e + CO_2(00^0 01) \leftrightarrow e + CO_2(00^0 11)$. For the initial asymmetric vibrational mode, i can be equal to 0, 1, 2, 3 and the final one j to 2, 3, 4, 5. The Fridman approximation scales the magnitude of the rate coefficients according to two parameters, α_f and β. Due to lack of data for excitation from $CO_2(v_1v_2{}^{l2}11)$ to higher levels, we have no information of the β value and for simplicity we use $\beta = 0$, i.e. the cross section σ_{12} has the same magnitude as σ_{01}, and $\alpha_f = 0.5$ [26]. To avoid an overpopulation of the vibrational distribution associated to the higher levels ($v_3 \geqslant 3$) of the asymmetric mode of CO_2, we investigated the possibility of setting α_f to 3 in expression (6) for the transitions $e + CO_2(v_1v_2{}^{l2}v_{3'}1) \leftrightarrow e\ CO_2(v_1v_2{}^{l2}v_31)$ with $v_3 = 3$, 4 and 5. Indeed, we saw unrealistically high populations of $v_3 = 3$, 4, 5 when using $\alpha_f = 0.5$ for all transitions while the calculated vibrational distribution functions (VDFs) were in good agreement with experimental ones, obtained using the FTIR setup described in the experimental section, when using $\alpha_f = 3$ for $v_3 \geqslant 3$. Note that this overpopulation is also strongly dependent on the scaling law used to describe the V-V rates. Using the cross sections from Laporta *et al* [60] for the asymmetric mode v_3, calculated only for resonant transitions, does not improve the results because non resonant contributions also play an important role, as stated in [60]. Setting α_f to 3 for higher levels improves the shape of the VDF and leads to a good agreement between the vibrational temperatures from the model and from the experiment but it means that the corresponding rate coefficients become very small. An investigation of the influence of the e-V processes on the VDF will be carried out in a future work but for this study we use $\alpha_f = 3$ for the transitions $e + CO_2(v_1v_2{}^{l2}v_{3'}1) \leftrightarrow e\ CO_2(v_1v_2{}^{l2}v_31)$ with $v_3 = 3$,4 and 5. However, note that the use of the Fridman approximation might not be adequate for the CO_2 molecules, as it was first introduced as a fit for the vibrational excitation rate coefficients of N_2 molecules. This may also justify the fact that we had to change the α_f, to describe the excitation of CO_2. Note that in table 1 of [18], the Fridman approximation is applied as (6) and only for the reactions number 7–10. For the other reactions, the cross sections are obtained according to the description in the dedicated column from the original cross sections available in [28]. The rate coefficient of the reverse processes is calculated from the principle of the detailed balance by multiplying the coefficients of the direct processes times the ratio of the statistical weights of the final and initial states and by the Boltzman factor $e^{-\Delta E/k_B \cdot T_e}$, where T_e is the electron temperature [61]. The list of all the e-V processes and corresponding cross sections for CO_2 are reported in the Supplementary Information. The processes for which cross sections are not available are also specified and the Fridman approximation was used in this case as explained above.

For the electron impact excitation of the CO vibrations, we have adopted the cross sections from [29] for the vibrational excitation and de-excitation which are largely based on resonant excitation data from Laporta *et al* [62], and where contributions from non-resonant collisions for the transition $e + CO(v = 0) \leftrightarrow e + CO(v = 1)$, taken from [47], are also included.

3.3.2. Vibrational quenching on the wall. An important phenomenon in the vibrational kinetics of CO_2 in our experimental conditions is the deactivation of vibrationally excited CO_2 and CO molecules through collisions on the wall having a significant influence on the vibrational characteristic temperatures especially for pressures below 1 Torr [20].

Following [20] and due to the lack of experimental data, we chose as default value of deactivation probability, γ_v, for any mode of CO_2 being deactivated to the ground state, $\gamma_v(CO_2(v > 0)) = 0.2$, for a Pyrex surface (average value from table 1 of [63]). We use a constant value of 4×10^{-2} for the deactivation probability for all levels of CO [63], which is significantly lower than for CO_2, as measurements showed that the probabilities of heterogeneous relaxation of CO do not depend on the value of v, at least for $v = 1$, 2 and 3 [64]. A certain dependence on the vibrational level could be expected, similar to the case of N_2, where a linear dependence of γ_v with the vibrational level is reported [65, 66]. Moreover, as opposed to CO_2, we consider single-quantum transitions as done for N_2 and O_2 in [42], where only one vibrational quantum is lost upon collision with the wall. No significant difference in the vibrational kinetics is expected for vibrational levels

below $v = 10$ between the assumption of single and multi-quanta relaxation. However, for higher vibrational levels, the best agreement of modelled and experimental CO VDFs was achieved for the 'multi-quanta' mechanism (loss of all vibrational quanta upon collision) [67].

3.3.3. V-V and V-T processes. One of the problems arising in the development of a state-to-state CO_2 model is the scarcity of data on the rate coefficients of different kinds of vibrational energy transitions within and between modes. For diatomic molecules, there are two main mechanisms of vibrational relaxation, namely, V-V exchanges of vibrational quanta and V-T transitions of vibrational energy to translation. However, since CO_2 is a polyatomic molecule, it has multiple vibrational modes and several additional relaxation channels like the inter-mode exchanges. Studying the vibrational kinetics of CO_2 thus requires a larger amount of data than for diatomic molecules.

Most of the data used for the V-T and V-V rate coefficients in our model are taken from the report of Blauer and Nickerson [68] regrouping experimental results and theoretical studies for the most important deactivation channels. This work provides rate coefficients (based on either experimental values or theoretically calculated results) for the first 14 vibrational levels of CO_2 ($v_1{}^{\max} = 2$, $v_2{}^{\max} = 5$, $v_3{}^{\max} = 1$). The authors have adapted the well-known SSH theory to the case of CO_2 vibrational energy transfers by considering the presence of Fermi resonance. Therefore, this report offers many rate coefficients for transitions involving changes for the v_1 or v_2 quantum numbers, while v_3 remains constant. Unfortunately, this is not sufficient for the description of transitions involving higher v_3 vibrational quantum number. For the missing reactions that cannot be found in literature, we determine the rate coefficients based on either SSH (Schwartz, Slawsky, Herzfeld) theory [69] or Sharma–Brau (SB) scaling [70] accounting for short-range contributions or describing transitions dominated by long-range interactions, respectively and ensuring that the obtained rate coefficients are not larger than the gas kinetic collision frequency (2.4×10^{-10} cm^{3}s^{-1} for CO_2 at 300 K [71]). However, note that the rate coefficients for collisionless V-V transfers can be higher than the gas kinetic collision processes as reported for SF_6 in [72]. This point is particularly relevant for the VV vibrational exchanges associated to CO_2 and more specifically to the intermode $VV(SB)_{CO2–CO2}$ which, in the literature, shows a rate coefficient of about 1.7×10^{-10}cm^{3}s^{-1} (according to experimental data in [73] at 298 K) and 2.1×10^{-10}cm^{3}s^{-1} (according to theoretical calculations in [74] at 300 K) very close (already for the first transition [73]) to the gas kinetic rate. Unlike the e-V processes described in the previous subsection, the V-V and V-T rates are derived only for single quantum exchanges and the complete set of V-T and V-V reactions for CO_2 can be found in Silva *et al* [17]. The reasons are that the databases for multi-quanta exchanges are too scarce and no experimental data is available for comparison and that the SSH and SB theories cannot predict a rate coefficient for these exchanges, while the forced harmonic oscillator (FHO) calculations from [66] confirm that for the low gas temperatures pertinent to this study multi-quanta transitions can be safely disregarded. More information on these processes can be found in a recent study on the vibrational kinetics of CO_2 [41].

All the processes included in the model are listed here and are detailed in the following sections:

$$\mathrm{VT_{CO2-CO2}}: \mathrm{CO_2}(v_1 v_2{}^{l2} v_3 f) + \mathrm{CO_2} \leftrightarrow \mathrm{CO_2}(v_1' v_2'{}^{l2'} v_3' f) + \mathrm{CO_2}$$

$$\mathrm{VT_{CO2-CO}}: \mathrm{CO_2}(v_1 v_2{}^{l2} v_3 f) + \mathrm{CO} \leftrightarrow \mathrm{CO_2}(v_1' v_2'{}^{l2'} v_3' f) + \mathrm{CO}$$

$$\mathrm{VT_{CO2-O2}}: \mathrm{CO_2}(v_1 v_2{}^{l2} v_3 f) + \mathrm{O_2} \leftrightarrow \mathrm{CO_2}(v_1' v_2'{}^{l2'} v_3' f) + \mathrm{O_2}$$

$$\mathrm{VV_{CO2-CO2}}: \mathrm{CO_2}(v_1 v_2{}^{l2} v_3 f) + \mathrm{CO_2}(v_1 v_2{}^{l2} v_3 f) \leftrightarrow \mathrm{CO_2}(v_1' v_2'{}^{l2'} v_3' f) + \mathrm{CO_2}(v_1'' v_2''{}^{l2''} v_3'' f)$$

$$\mathrm{VV(SB)_{CO2-CO2}}: \mathrm{CO_2}(v_1 v_2{}^{l2} v_3 f) + \mathrm{CO_2}(v_1 v_2{}^{l2} v_3 f) \leftrightarrow \mathrm{CO_2}(v_1 v_2{}^{l2}(v_3+1) f) + \mathrm{CO_2}(v_1 v_2{}^{l2}(v_3-1) f)$$

$$\mathrm{VT_{3-O}}: \mathrm{CO_2}(00^{\circ} v_3 1) + \mathrm{O} \leftrightarrow \mathrm{CO_2}(0(v_2 = 2,3,4)^{2,3,4}(v_3-1)1) + \mathrm{O}$$

$$\mathrm{VT_{2-O}}: \mathrm{CO_2}(0 v_2{}^{l2} 01) + \mathrm{O} \leftrightarrow \mathrm{CO_2}(0(v_2{}^{l2-1}-1)01) + \mathrm{O}$$

$$\mathrm{VV_{3-CO}}: \mathrm{CO_2}(v_1 v_2{}^{l2}(v_3+1) f) + \mathrm{CO}(w) \leftrightarrow \mathrm{CO_2}(v_1 v_2{}^{l2} v_3 f) + \mathrm{CO}(w+1)$$

$$\mathrm{VV_{1,2-CO}}: \mathrm{CO_2}(\left(v_1+1)(v_2+1)^{l2+1} v_3 f\right) + \mathrm{CO}(w) \leftrightarrow \mathrm{CO_2}(v_1 v_2{}^{l2} v_3 f) + \mathrm{CO}(w+1)$$

$$\mathrm{VV_{CO-CO}}: \mathrm{CO}(v) + \mathrm{CO}(w-1) \leftrightarrow \mathrm{CO}(v-1) + \mathrm{CO}(w)$$

$$\mathrm{VT_{CO-CO}}: \mathrm{CO}(v) + \mathrm{CO} \leftrightarrow \mathrm{CO}(v-1) + \mathrm{CO}$$

$$\mathrm{VT_{CO-CO2}}: \mathrm{CO}(v) + \mathrm{CO_2} \leftrightarrow \mathrm{CO}(v-1) + \mathrm{CO_2}$$

$$\mathrm{VT_{CO-O2}}: \mathrm{CO}(v) + \mathrm{O_2} \leftrightarrow \mathrm{CO}(v-1) + \mathrm{O_2}$$

$$\mathrm{VT_{CO-O}}: \mathrm{CO}(v) + \mathrm{O} \leftrightarrow \mathrm{CO}(v-1) + \mathrm{O}$$

3.3.3.1. CO_2- CO_2 V-V/V-T. There are roughly 350 V-T and 600 V-V direct processes to describe the kinetics of the 72 CO_2 vibrational states considered. The various coefficients are fitted through the following exponential expression [68]:

$$k\left(\mathrm{cm^3 s^{-1}}\right) = 1{,}66 \times 10^{-24} \times \exp\left(a + b \times T^{-1/3} + c \times T^{-2/3}\right) \quad (7)$$

where a, b and c are the fitting constants. The rate coefficients for the inverse reactions are calculated by the principle of detailed balance [61].

The transitions involving higher vibrational levels are scaled with the SSH theory, except for the nearly resonant collisional up-pumping process along the asymmetric stretching mode, given by:

$$\mathrm{CO_2}\left(00^{\circ}\mathrm{v_3}1\right) + \mathrm{CO_2}\left(00^{\circ}\mathrm{v_3}1\right) \leftrightarrow \mathrm{CO_2}\left(00^{\circ}\left(\mathrm{v_3}-1\right)1\right) + \mathrm{CO_2}\left(00^{\circ}\left(\mathrm{v_3}+1\right)1\right)$$

In this case, the SB theory (based on long-range forces) was used (instead of SSH) to obtain an empirical formula for the rate constants as a function of the gas temperature for ($T_g < 1200$ K) from the rate coefficient determined experimentally at 298 K ($1.7 \times 10^{-10}\mathrm{cm^3 s^{-1}}$) [73]. According to this theory, the rate coefficient decreases with the increase of the gas temperature and is valid for gas temperatures below 1000 K. To avoid rate coefficients corresponding to a probability higher than 1 as recommended in [17], we use the same rate coefficient for all transitions with $v_3 > 1$. To verify that the transition probabilities obtained are lower than 1 we calculate the reaction rates with the gas–kinetic collision frequency, obtained for a hard sphere model as [42],

$$\nu_{\mathrm{collision}} = \sqrt{\frac{8 \cdot k_B \cdot T_g}{\pi \cdot \mu}} \cdot \pi \cdot R^2, \quad (8)$$

with μ is the reduced mass of the colliding particles (taken as 3.65×10^{-26} kg), R is the distance of collision assumed to be the Lennard Jones potential distance (taken as 3.763×10^{-10} m [75]), k_B is the Boltzmann constant and T_g is the gas temperature. Note however that rate coefficients calculated using the SB theory can in fact get larger than the gas kinetic collision rates because they are due to long range interaction [70].

3.3.3.2. CO_2-O V-T. The quenching of vibrationally excited CO_2 by O atoms is taken into account following the atmospheric model from López-Puertas *et al* [76, 77]. Two different mechanisms are considered here:

$\mathrm{VT_{3\text{-}O}}$: $\mathrm{CO_2}(00^{\circ}v_3 1) + \mathrm{O} \leftrightarrow \mathrm{CO_2}(0(v_2 = 2{,}3{,}4)^{2,3,4}(v_3\text{-}1)1) + \mathrm{O}$ with a rate coefficient for the forward direction, for $\nu_3 = 1$, given as:

$$k\left(\mathrm{cm^3 s^{-1}}\right) = 2 \times 10^{-13} \times \left(\frac{T}{300}\right)^{1/2} \quad (9)$$

$\mathrm{VT_{2\text{-}O}}$: $\mathrm{CO_2}(0v_2{}^{l2}01) + \mathrm{O} \leftrightarrow \mathrm{CO_2}(0(v_2{}^{l2-1}\text{-}1)01) + \mathrm{O}$ with a rate coefficient for the forward direction given as:

$$k\left(\mathrm{cm^3 s^{-1}}\right) = \left(2.32 \times 10^{-9} \exp\left(-76.75 \cdot T^{-1/3}\right) + \left(1 \cdot 10^{-14} \cdot T^{1/2}\right)\right). \quad (10)$$

Both rate coefficients are scaled with a harmonic oscillator scaling (linear with ν) for ν_3 and $v_2 > 1$ according to [11]. At 300 K we obtain for $\mathrm{VT_{3\text{-}O}}$ 2×10^{-13} $\mathrm{cm^3 s^{-1}}$ and for $\mathrm{VT_{2\text{-}O}}$ 1.98×10^{-13} $\mathrm{cm^3 s^{-1}}$ comparable to the values of 2.08×10^{-13} $\mathrm{cm^3 s^{-1}}$ and 1.89×10^{-13} $\mathrm{cm^3 s^{-1}}$ obtained experimentally using laser fluorescence techniques respectively by Buchwald and Wolga [78] and Cramp and Lambert [79]. Concerning higher temperatures, at 3000 K for instance we calculate for $\mathrm{VT_{3\text{-}O}}$ 6.3×10^{-13} $\mathrm{cm^3 s^{-1}}$ and $\mathrm{VT_{2\text{-}O}}$ 1.2×10^{-11} $\mathrm{cm^3 s^{-1}}$, to compare against the shock tube data 3.8×10^{-12} $\mathrm{cm^3 s^{-1}}$ obtained in [80] where the vibrational relaxation of the bending mode of CO_2 by O atoms was measured in the temperature range of 2000 K – 4000 K by infrared emission measurements. Expressions (9) and (10) can thus be used with confidence for a temperature range of $300 < Tg < 1000$ K and should be used with care for higher temperatures. However, note that Castle *et al* [81] reviewed values for the rate coefficient corresponding to $\mathrm{VT_{2\text{-}O}}$ found in the literature in the range $1.2 - 6 \times 10^{-12}$ $\mathrm{cm^3 s^{-1}}$ which is roughly one order of magnitude higher than what is reported in [76–79].

3.3.3.3. $CO_2(v)$-M and CO(v)-M V-T. A possible way to obtain the $\mathrm{CO_2}(v)$-M (M = CO, $\mathrm{O_2}$) V-T rate coefficients is to multiply the known $\mathrm{CO_2}(v)$-$\mathrm{CO_2}$ coefficients by the constant'relative efficiency' factor Φ suggested in [68]. However, a more general approach is to scale the rate coefficients with a non-constant factor Φ calculated according to the theoretical dependences from the SSH theory on the vibrational levels and gas temperature, as done in [42] for $\mathrm{N_2}(v)$-$\mathrm{O_2}$ and in [20] for $\mathrm{N_2}(v)$-$\mathrm{CO_2}$ energy transfers calculated from the V-T $\mathrm{N_2}(v)$-$\mathrm{N_2}$. This approach was adopted for $\mathrm{CO}(v)$-M (M = $\mathrm{CO_2}$, $\mathrm{O_2}$) V-T and $\mathrm{CO_2}(v)$-M (M = CO, $\mathrm{O_2}$) V-T for which we used, respectively, the known rate coefficients of CO(v)-CO V-T (described in the next section) and of $\mathrm{CO_2}$(v)-$\mathrm{CO_2}$ V-T described in [17].

3.3.3.4. CO-CO V-T. The rate coefficients for the V-T transfers between CO molecules $\mathrm{CO}(v) + \mathrm{CO} \leftrightarrow \mathrm{CO}(v\text{-}1) + \mathrm{CO}$ taken from [82] were fitted for each vibrational quantum number with the gas temperature (K) using the following expression:

$$k\left(\mathrm{cm^3 s^{-1}}\right) = T_g^p \times \exp\left(a \times T_g^{-1} + b \times T_g^{-1/3} + c \times T_g^{-2/3} + d \times T_g^{-4/3} + e \times T_g^{-5/3}\right) \text{for} \; 200 < T_g < 2000 \quad (11)$$

with a, b, c, d, e and p fitting parameters depending on the vibrational level v reported in table 4 and T_g the gas temperature.

The rate coefficients obtained through the fitting of the data from Cacciatore and Due Billing [82], as explained above, are in good agreement with the original data, as can be seen in

Table 4. Fitting parameters corresponding to the coefficients in expression (11) for the determination of the rate coefficient of the processes CO(v) + CO ↔ CO(v-1) + CO depending on the vibrational level v.

v	*p*	*a*	*b*	*c*	*d*	*e*
1	−15.7	1369 066.1	7062.1	−152 282.5	−5728 820.0	9109 363.3
2	−17.4	1676 528.2	8208.4	−180 552.3	−7307 224.3	12 219 240.7
3	−17.4	1774 248.6	8428.4	−188 018.3	−7868 692.9	13 406 893.1
4	−16.8	1782 710.7	8268.5	−186 764.9	−7993 304.5	13 765 067.3
5	−16.0	1756 422.0	7973.8	−182 242.0	−7943 995.6	13 789 509.0
6	−15.1	1711 488.3	7615.6	−176 048.2	−7798 579.8	13 626 437.5
7	−14.1	1655 326.2	7225.5	−168 912.3	−7593 034.4	13 343 357.2
8	−13.2	1592 228.9	6821.4	−161 251.1	−7348 313.0	12 979 633.9
9	−12.3	1524 967.7	6414.5	−153 330.1	−7078 047.8	12 560 968.5
10	−11.5	1455 436.6	6012.2	−145 327.9	−6791 643.7	12 105 186.1

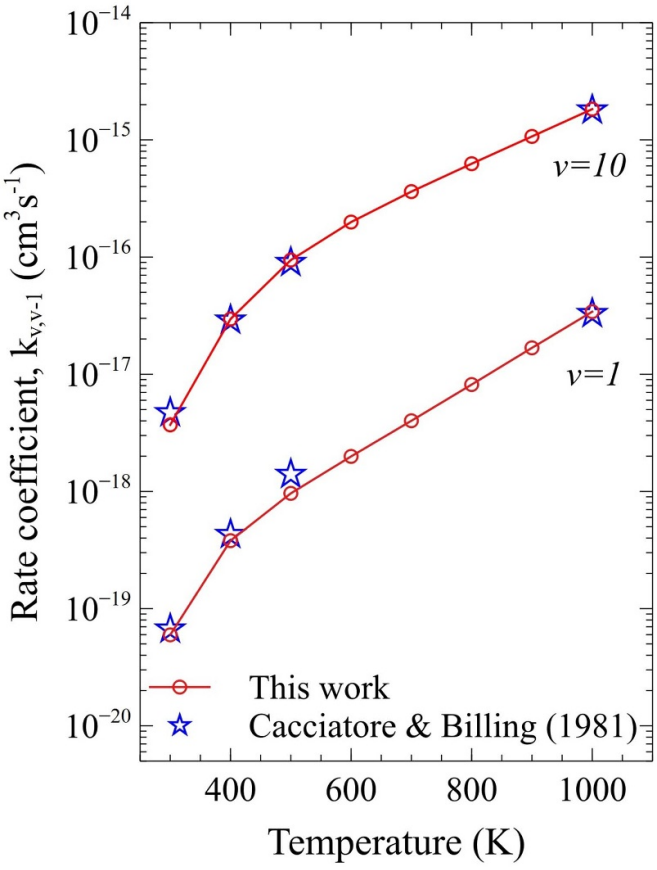

Figure 1. Rate coefficients for the reaction CO(v) + CO → CO(v − 1) + CO as a function of the gas temperature. Data from [76] (☆) and fit (o).

figure 1, especially between 300 K and 1000 K which corresponds to the range of gas temperatures measured for our conditions.

3.3.3.5. CO-O V-T. The quenching of vibrationally excited CO by O atoms is included as described in [61], with an Arrhenius type temperature dependence:

$$k_{10}\,(\mathrm{CO}-\mathrm{O})\left(cm^3s^{-1}\right) = 5.3\ \times\ 10^{-13}\cdot T_g^{1/2}\cdot\exp\left(-\tfrac{1600}{T_g(K)}\right) \tag{12}$$

and the harmonic oscillator scaling is assumed for $v > 1$.

3.3.3.6. CO-CO V-V. We include 90 V-V processes in our model for $0 < v < 10$ and we chose the results of the trajectory calculations from Cacciatore and Due Billing [82] as a reference. Indeed, the rate coefficients obtained from their calculations were in good agreement with experimental data between 100 and 500 K and for vibrational levels up to 10 or more. However, only 24 processes are present in [82] and we thus need to scale the missing rate coefficients. To obtain a closed expression that approximates the results of Cacciatore and Due Billing [82] for the temperature range of interest here, we start from the FHO parametrization by Plönjes *et al* [83]. Note that it is necessary to multiply the obtained rate coefficient by a factor $Z\left(\mathrm{cm^3s^{-1}}\right) = 3\ \times\ 10^{-10}\ \times\ \left(\frac{T}{300}\right)^{1/2}$ to derive the overall rate coefficient.

To improve the agreement with the calculated rate coefficients from Cacciatore and Due Billing [82], we use the approximation of the adiabaticity factor (corresponding to $\lambda^{v,v-k}_{w-k,w}$ in [83]) given in [42] for which we consider the characteristic length $L = 1\ \times\ 10^{-11}$ m similarly to the N_2–N_2 and N_2–O_2 systems where Guerra *et al* [42] used $L = 2\ \times\ 10^{-11}$ m and $L\ =\ 3\ \times\ 10^{-11}$ m, respectively. We use a constant rate coefficient $8.85\ \times\ 10^{-13}\mathrm{cm^{-3}s^{-1}}$ taken from [82] (average of rate coefficients from 100 K to 1000 K) for the first process $\mathrm{CO}(v=0) + \mathrm{CO}(v=1) \rightarrow \mathrm{CO}(v=1) + \mathrm{CO}(v=0)$.

Finally, using the rate coefficient of the process $\mathrm{CO}(v=1) + \mathrm{CO}(v=1) \rightarrow \mathrm{CO}(v=0) + \mathrm{CO}(v=2)$ from [82] we renormalize the rate coefficient calculated from the procedure in Plönjes *et al* [83]. We used a double exponential to fit the ratio between the rate coefficients from [82, 83] dependent on the gas temperature and following the expression:

$$a\times\exp\left(b\times T\right) + c\times\exp\left(d\times T\right) \tag{13}$$

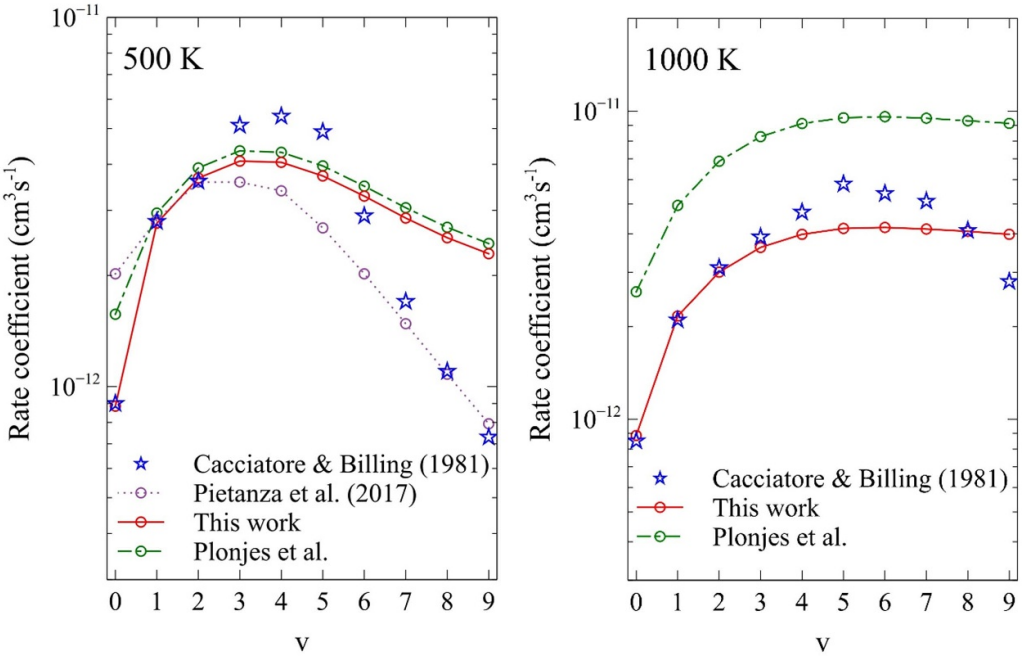

Figure 2. Rate coefficients for the non-resonant process: CO(1) + CO(v) → CO(0) + CO(v + 1) at 500 K (left) and 1000k (right) as a function of v used in this work (—) compared with the results from López-Puertas *et al* [76](☆), Buchwald *et al* [78] (···) and obtained from the expression in Castle *et al* [81] (-·-) before correction (see equation (13)).

with $a = 2.088$, b=−0.0018, $c = 0.08784$ and $d = 0.000041$. This correction was necessary to get a good temperature dependence of the rate coefficients as can be seen in figure 2.

In figure 2, the rate coefficients for the non-resonant process, CO(1) + CO(v-1) → CO(0) + CO(v), are plotted as a function of ν, at 500 K and 1000 K, and compared with the results from Cacciatore and Due Billing [82] and Pietanza *et al* [84].

Some rate coefficients are shown as a function of the gas temperature on figure 3. The agreement is very good between the rate coefficients determined in this work and the ones computed by Cacciatore and Due Billing [82] for low vibrational levels and remains satisfactory even for higher vibrational levels.

3.3.3.7. CO_2-CO V-V. As pointed out in the introduction, the transfers between vibrationally excited CO and the asymmetric stretch mode of CO_2 are very efficient and can promote the ladder climbing mechanism along this CO_2 mode, with a potential positive effect on CO_2 dissociation. CO molecules can transfer a considerable amount of energy to the v_3 vibration because the difference between the energies of the first vibrational level of CO and the $(00^0 11)$ level of CO_2 is only 170 cm^{-1}, which is smaller than the average kinetic energy kT [85]. Moreover, the observed cross sections of excitation of molecular vibrations of CO are unusually large, which is related to the resonance effect of short-lived negative ions CO^- [86].

Kustova *et al* [87] provide a straightforward procedure to obtain accurate rate coefficients for the V-V transfer between CO_2 and CO.

$$\begin{aligned}
&\mathrm{VV}_{3-\mathrm{CO}}:\ \mathrm{CO_2}(v_1 v_2{}^{l2}(v_3+1)f) + \mathrm{CO}(w)\\
&\quad \leftrightarrow \mathrm{CO_2}(v_1 v_2{}^{l2} v_3 f) + \mathrm{CO}(w+1)\\
&\mathrm{VV}_{1,2-\mathrm{CO}}:\ \mathrm{CO_2}\left((v_1+1)(v_2+1)^{l2+1} v_3 f\right) + \mathrm{CO}(w)\\
&\quad \leftrightarrow \mathrm{CO_2}(v_1 v_2{}^{l2} v_3 f) + \mathrm{CO}(w+1)
\end{aligned}$$

The rate coefficients of vibrational energy transitions between the lowest vibrational states are computed using experimental data from [88] and can be calculated using the expression:

$$k_{0\to1} = \frac{k\cdot T}{P\cdot\tau},\ with\, P\cdot\tau = 10^{A_0 + A_1 T^{-1/3} + A_2 T^{-2/3}} \qquad (14)$$

The value of the A_n constants can be found in table 1 of [87]. The remaining rate coefficients (for higher states) are calculated on the basis of the harmonic oscillator modified for polyatomic molecules.

For $\mathrm{VV}_{3\text{-CO}}$, we use the scaling $k(w \to w+1)$ $(v_3 + 1 \to v_3) = k_{0\to1} * (v_3 + 1) * (w + 1)$.

For $\mathrm{VV}_{1,2\text{-CO}}$, we use the scaling $k(w \to w+1)$ $(v_{1,2} + 1 \to v_{1,2}) = k_{0\to1} * (v_1 + 1) * (v_2 + 1) * (w + 1)$.

We compared the values obtained in this work following the procedure from Kustova *et al* [87] for the process $CO_2(00°11)$ + CO(0) → $CO_2(00°01)$ + CO(1) with values determined experimentally by Rosser *et al* [89] (linear dependence between 300 and 900 K within experimental error), Starr and Hancock [90] and Blauer and Nickerson [68] and found a good agreement, as shown in figure 4.

The rate coefficients of the reverse transitions are related to the rate coefficients of forward transitions by the detailed balance principle [61]. The collision frequency (or gas kinetic rate) represented in figure 5 along with a few calculated rate

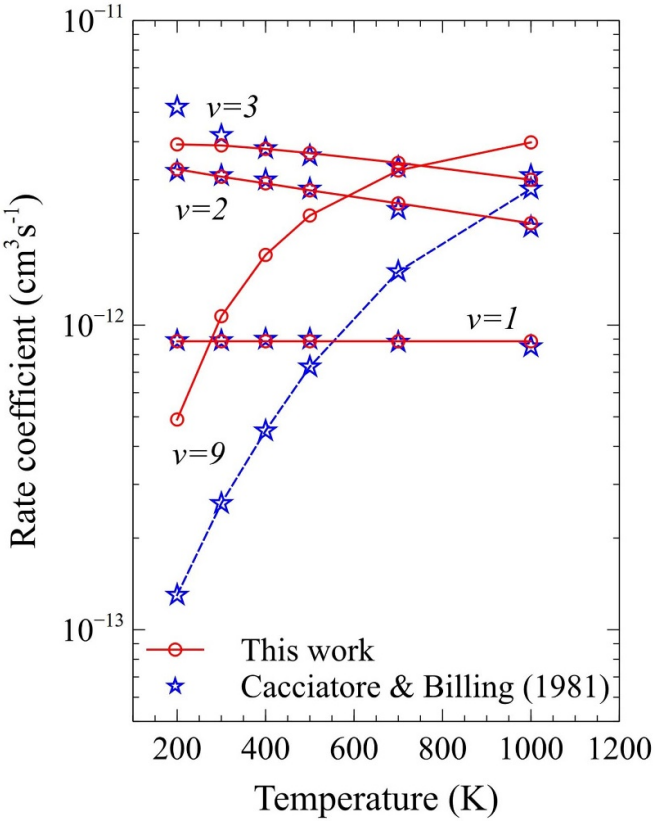

Figure 3. Rate coefficient for CO(1) + CO(v) → CO(0) + CO(v + 1) as a function of the gas temperature, compared with the results from López-Puertas *et al* [76].

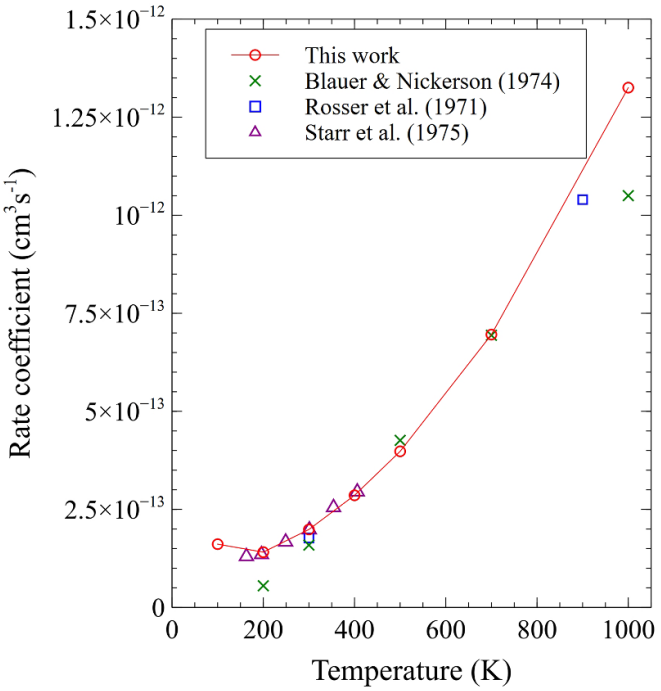

Figure 4. Rate coefficients for the process: $CO_2(00^\circ 11) + CO(0) \rightarrow CO_2(00^\circ 01) + CO(1)$ used in this work (—) against experimental results (symbols).

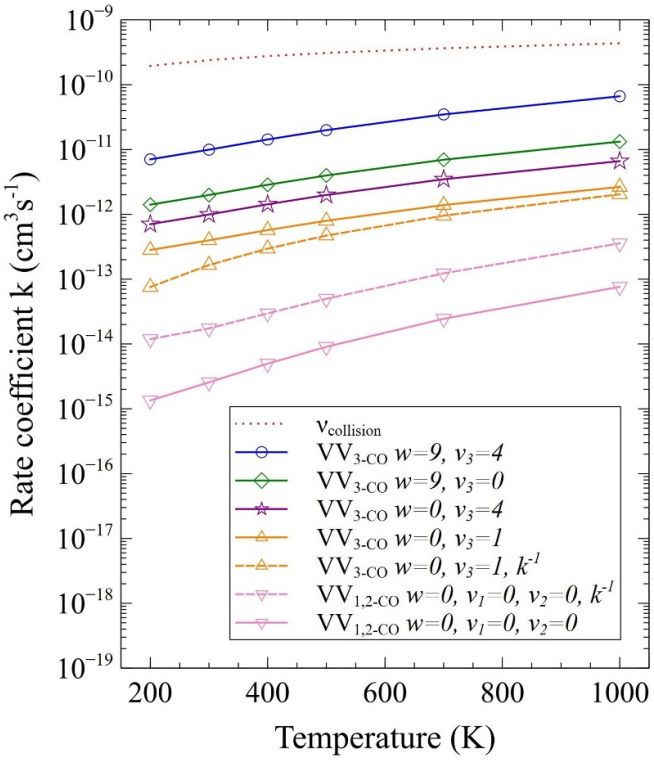

Figure 5. Rate coefficients for the direct and indirect (k^{-1}) processes:$CO_2(v_3 + 1) + CO(w) \leftrightarrow CO_2(v_3) + CO(w + 1)$ ($VV_{3\text{-}CO}$) and $CO_2(v_1 + 1,v_2 + 1) + CO(w) \leftrightarrow CO_2(v_1,v_2) + CO(w + 1)$ ($VV_{1,2\text{-}CO}$), and gas collision frequency $\nu_{collision}$ as a function of the gas temperature for different combination of v_1, v_2, v_3 and w (being equal to zero if not specified in the legend).

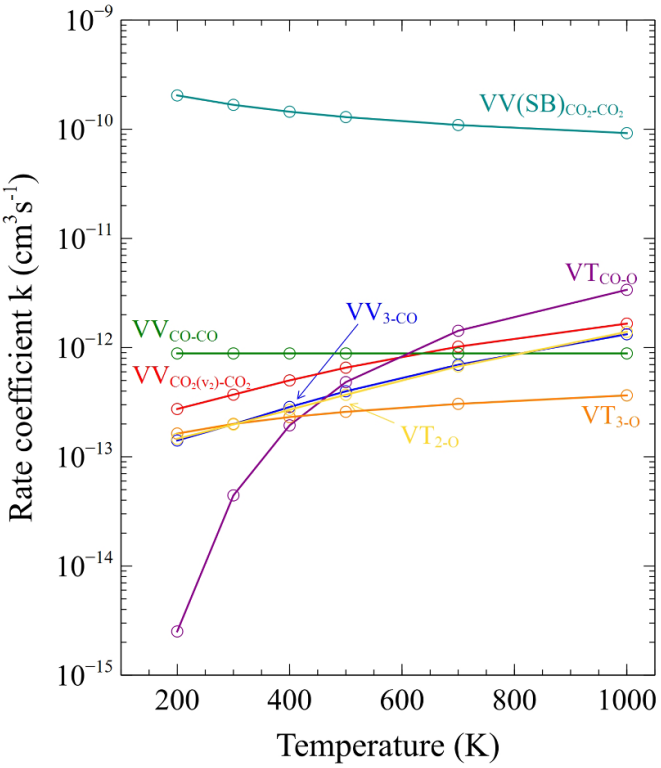

Figure 6. Rate coefficients of vibrational energy transitions between the lowest levels.

coefficients, is estimated via a hard sphere model (cf expression 8), gives an upper limit for the scaled rate coefficients and we ensure that no rate coefficient corresponds to a probability above 1.

3.3.3.8. Summary of the most important rate coefficients. The rate coefficients of vibrational energy transitions between the lowest states of several V-V and V-T processes are plotted in figure 6. The rate coefficients of these processes differ by several orders of magnitude. The most important ones in term of amplitude are the quenching of vibrationally excited CO_2 and CO molecules by atomic oxygen ($VT_{3\text{-}O}$ and $VT_{CO\text{–}O}$) and the vibrational-to-vibrational transfer between two CO_2 molecules ($VV(SB)_{CO2\text{–}CO2}$), two CO molecules ($VV_{CO\text{–}CO}$) and finally the vibrational transfer between CO and CO_2 ($VV_{3\text{-}CO}$).

4. Results and discussion

The results of the model are compared with experimental measurements of the fraction of atomic oxygen, reduced electric field, dissociation fraction of CO_2 and vibrational temperatures of CO_2 and CO in a DC reactor at pressures between 0.4 and 5 Torr (53.33–666.66 Pa). This comparison provides the validation of the model, as well as the interpretation of the measured quantities and the identification of the main processes ruling the discharge. In our conditions, we can assume that T_{rot} is in equilibrium with the gas temperature and is used as an input parameter for the model. Moreover, since the characteristic temperatures corresponding to the effective symmetric mode, T_1, (which includes the Fermi resonant states) and bending mode, T_2, in our conditions, are nearly the same, we define a common temperature of the bending and symmetric stretching modes denoted $T_{1,2}$ [18, 35]. This comes from the occurrence of the Fermi resonance between the symmetric and bending modes of vibration and with the similarity of the energies and rate coefficients involving Fermi and non-Fermi bending levels. Therefore, the two characteristic temperatures $T_{1,2}$ and T_3 are enough for a simple description of the extent of vibrational excitation although this is not imposed in the model.

Besides, it is worth noting that our state-to-state model provides the populations of each individual vibrational levels of the different modes of CO_2 and of CO. Therefore, the vibrational temperature is calculated, assuming a Treanor distribution [91], as:

$$T_{v,ij} = \left(\frac{E_1}{\ln(p_i/p_j) - \frac{E_j - E_i - E_1}{k_B \cdot T_g}} \right) \Big/ k_B \qquad (15)$$

where E_1 is the energy of the first v_3 level, $(00^{0}11)$, for T_3, or of the first v_2 level, $(01^{1}01)$, for $T_{1,2}$, and p_i and p_j and E_i and E_j are the populations and energies of levels i and j, respectively. We use an average of the two temperatures calculated using the first three vibrational levels of each mode: for the asymmetric stretch mode the two couples (i,j) used for the averaging are $v_3 = (0,1)$ and $(1,2)$ (with $v_1 = v_2 = 0$)); similarly, for the determination of $T_{1,2}$ we use the pure bending mode and the couples $v_2 = (0,1)$ and $(1,2)$ (with $v_1 = v_3 = 0$)). Finally, T_g is the gas temperature and k_B the Boltzmann constant.

4.1. Validation of the CO vibrational kinetics and effect of the wall deactivation

This section focuses on the validation of the CO vibrational kinetics by comparing the simulations results with experimental data obtained in a DC glow discharge ignited in 100% CO_2 in a Pyrex tube of radius 1 cm and 67 cm length, for a current of 40 mA as described in details in [35].

In figure 7 the measured and calculated common vibrational temperature of the CO_2 bending and symmetric modes $T_{1,2}$, the vibrational temperature of the asymmetric stretching mode T_3, the CO vibrational temperature T_{CO}, the rotational temperature T_{rot}, the reduced electric field and the fractions of atomic oxygen and CO are presented. These two last quantities show a very good agreement between calculations and measurements. The self-consistently calculated reduced electric field is overestimated for all conditions and a few reasons for this discrepancy are discussed in section 4.3. The CO vibrational kinetics scheme added to the model are able to successfully reproduce the measured T_{CO} values within an error of 10%, we can therefore consider that our CO vibrational kinetic scheme is validated. Overall, all calculated quantities are in very good agreement with the experimental data and more specifically, for the temperatures, when the wall deactivation of vibrations is included.

The influence of deactivation of vibrationally excited CO_2 and CO at the walls, described in section 3, is illustrated in figure 7, for the case of pure CO_2. Including the wall deactivation for vibrationally excited CO_2 and CO molecules mostly affects the vibrational temperatures of these molecules but not the other quantities like O/N, CO/N and *E/N*. T_{CO}, $T_{1,2}$ and T_3 decrease for all conditions and the trends as a function of the pressure are improved and leading to a better agreement with the measurements. The results change drastically in the case of a discharge below 2 Torr, while they are very similar at higher pressures, as expected, and also observed in [20]. Moreover, we could observe that including the detailed balance for the wall deactivation processes only affected $T_{1,2}$, up to 7% increase for the lowest pressure. In turn, the influence on T_3 and T_{CO} remains below 0.3%. The default deactivation probabilities of the different modes of CO_2 lead to calculated $T_{1,2}$ values lower than in the experiment. Since no experimental values for the wall deactivation probability (on Pyrex) of the bending mode of CO_2 were reported in the literature to our knowledge, we thus propose a deactivation probability for the bending, symmetric stretch, and mixed modes of

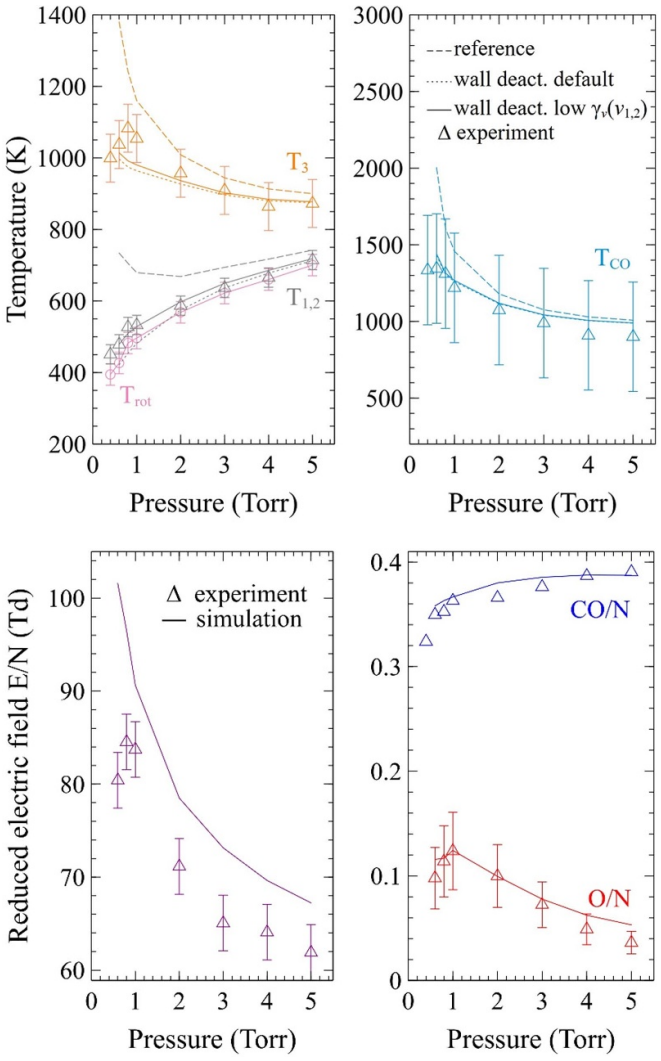

Figure 7. Experimental values (Δ) and calculated values (line) of the common vibrational temperature of the CO_2 bending and symmetric modes $T_{1,2}$, the vibrational temperature of the asymmetric stretching mode T_3, the CO vibrational temperature T_{CO}, the rotational temperature T_{rot} (measured), the reduced electric field E/N, and the CO and O fractions, CO/N and O/N, when a discharge is ignited in CO_2, at current = 40 mA and as a function of pressure. The model calculations were done including with the default probabilities from section 3.3. (···), $\gamma_v(v_{1,2}) = 0.05$ (—) and excluding (——) the wall deactivation of the vibrationally excited states of CO and the different modes of CO_2, at the wall.

0.05 instead of 0.2 and this corresponds to the results labelled $\gamma_v(v_{1,2}) = 0.05$ in figure 7.

4.2. Effect of atomic oxygen on the vibrational kinetics of CO_2 and CO

In order to study the effect of the quenching of vibrational energy by O atoms as a function of the O_2 content we have reproduced with our model the experimental conditions discussed in [34]. These conditions are: (a) similar to those previously described in this work, more specifically, a CO_2 gas discharge is ignited in a cylindrical Pyrex tube of 1 cm radius

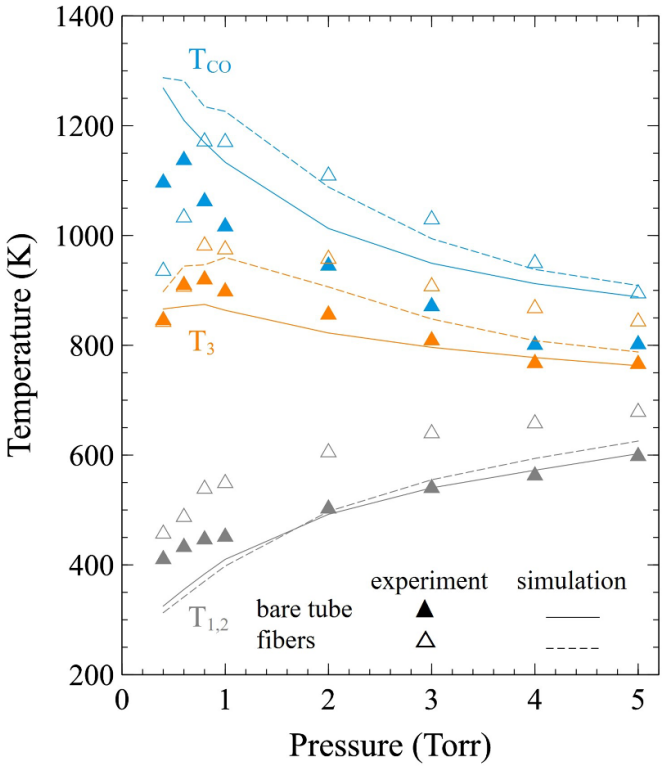

Figure 8. Experimental values (Δ) and calculated values (line) of the common vibrational temperature of the CO_2 bending and symmetric modes $T_{1,2}$, the vibrational temperature of the asymmetric stretching mode T_3 and the CO vibrational temperature T_{CO}, for a pure CO_2 discharge, at current = 20 mA. The O loss probability γ_O obtained experimentally in [35] is used in our calculations for the case of the bare Pyrex tube (—) and γ_O is set to 1 to reproduce the case of the tube covered with fibers (—).

and tube length of 23 cm at a current of 20 mA. For this condition, the atomic oxygen recombination probabilities γ_O used are taken from [35]. Finally, the gas temperature used for the simulations is not reproduced in figure 8 but can be found in [34]; (b) similar as before but with the inside of the Pyrex tube covered with a layer of micro-structured silica fibers, increasing the effective surface area in contact with the plasma to enhance the O atom recombination and consequently reduce the density of O atoms in the gas mixture, in which case we set $\gamma_O = 1$ for the simulations. The vibrational and rotational temperatures of CO_2 and CO were measured with *in situ* FTIR spectroscopy and atomic oxygen density and loss frequency by actinometry. Note that as a first estimation we assume a constant value of gamma ($\gamma_O = 1$) to capture the phenomenon, however a dependence with pressure could improve the agreement between simulation and experiment.

Figure 8 presents the vibrational temperatures calculated in the simulations and measured experimentally, in the case of the bare tube, corresponding to γ_O obtained from loss frequency measurements in [35] and for the tube covered with fibers, corresponding to $\gamma_O = 1$ in the simulations. As can be observed in figure 8, the different vibrational temperatures, from the calculations and experiments, as a function of the pressure, are in good agreement for T_3 and T_{CO}. The trend of T_3 with pressure seem to improve when using $\gamma_O = 1$ in the simulations, as the maximum around 1 Torr, observed in the experiments, is reproduced in the calculations. This shows the importance of the atomic oxygen heterogeneous recombination mechanism for an accurate description of the plasma at low pressure. The calculated $T_{1,2}$ is too low when compared with the experiments especially for the case with the fibers. $T_{1,2}$ from the simulations is almost thermalized with T_{rot} for both cases (with and without fibers) while in the experiment this is only observed for the bare tube. This could come, at least partly, from the wall deactivation, for which we use the default value presented in section 3.3, as it is the main quenching mechanism of $T_{1,2}$. However, to the best of our knowledge no experimental values for the wall deactivation probability (on Pyrex) of the bending mode of CO_2 were reported in the literature, making it difficult to address this question realistically. Since the depletion of vibrational levels of O_2 is dominated by the V-T process with O atoms [48] we would anticipate that the vibrations of O_2 might play a role in the case of the discharge with a low atomic oxygen fraction and that the V-V process CO_2 $(0v_2^{l2}01))+ O_2(v = 1)$ [92] could lead to the excitation of the bending mode therefore increasing the $T_{1,2}$. However, the O_2 vibrations are still have a negligible effect on the simulation results. A similar process with vibrationally excited O_3 [81] can occur but due to the low density of this species in the discharge it was verified that it does not play a role in our conditions. We conclude that the deactivation of the bending mode of CO_2 by V-T processes (including wall deactivation) is the rate determining step for the relaxation of CO_2. However, the rate coefficients for $CO_2(v_2)$-M V-T processes can vary by more than one order of magnitude depending on the [81, 93]. A more precise determination of these rate coefficients is necessary, as advocated in [94] and highlighted here.

The experimental results [34] show a remarkable increase of the vibrational excitation of both CO_2 and CO with the large surface material confirming that atomic oxygen is a strong quencher of the vibrations of both species. Besides, it was also verified that neither the dissociation fraction nor the reduced electric field were changing significantly, within the reproducibility error and that O atom density decreased drastically, down to ∼5% of the density measured with the bare tube.

Likewise, in the simulations, the dissociation fraction is only changing by around 0.05 and the reduced field by less than 2% while the fraction goes down to 0.7%–2.5% (depending on the pressure) of the reference O/N attesting than atomic oxygen does not participate in back reactions as stated in [34]. Besides, the increase of T_3 by 100 K (figure 8), in average, does not influence much the dissociation fraction and this proves that the vibrational kinetics are not playing a significant role in the dissociation of CO_2 in our experimental conditions. However, this study illustrates the important role of O atoms in the quenching of vibrations which is essential in these conditions and should not be overlooked.

4.3. Validation of the model for the CO_2–O_2 mixture

In this section we compare the results of our extended model with experimental data measured in a CO_2–O_2 DC discharge.

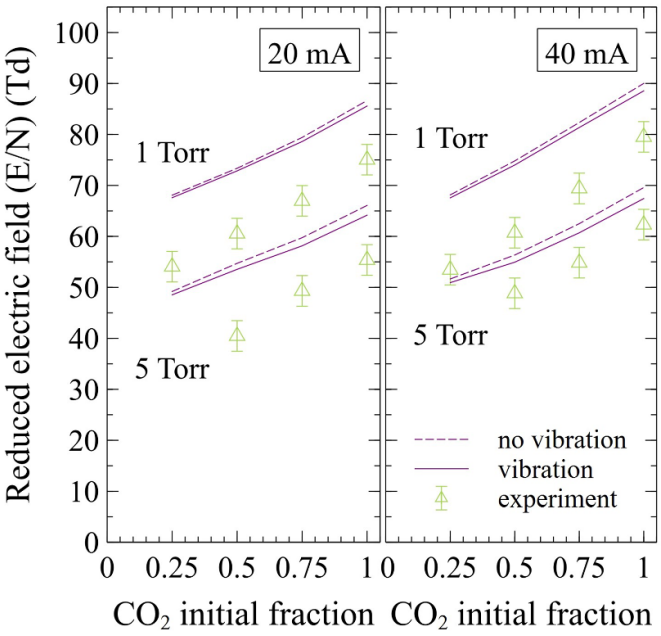

Figure 9. Reduced electric field E/N, of a CO_2-O_2 discharge as a function of the CO_2 initial fraction, at a current of 20 mA and 40 mA for 1 and 5 Torr: experiment (Δ), model calculations excluding (– –) and including (—) the vibrational kinetics in Loki C.

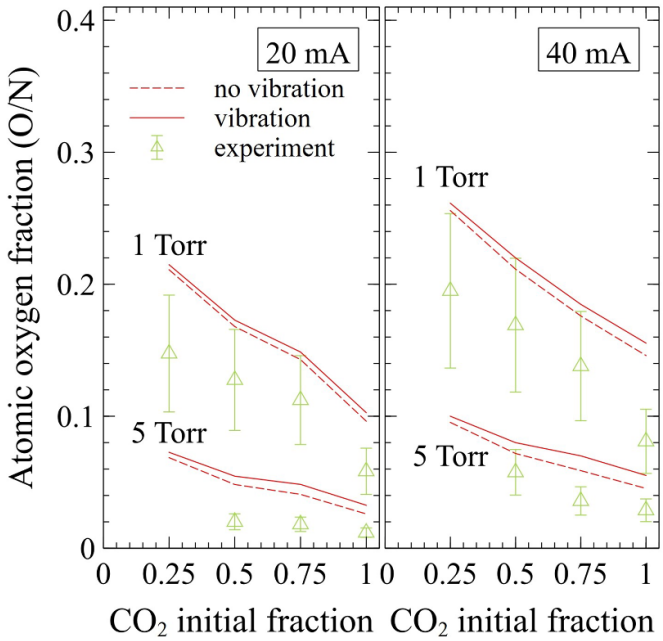

Figure 10. Atomic oxygen fraction O/N of a CO_2-O_2 discharge as a function of the CO_2 initial fraction, at a current of 20 mA and 40 mA for 1 and 5 Torr: experiment (Δ), model calculations excluding (– –) and including (—) the vibrational kinetics in Loki C.

The calculated reduced electric field, vibrational temperatures, atomic oxygen fraction and CO_2 dissociation fraction are compared with the measurements. The model shows a satisfactory quantitative agreement and reproduces very well the dependencies of the measured quantities for different pressures, discharge currents (input power) and initial CO_2 fractions in the CO_2–O_2 mixture. As mentioned in section 2, T_{rot} can be assumed to be in equilibrium with the gas temperature and it is used as an input parameter for the model. For the simulations presented in this section the gas temperature given as an input to the model is the T_{rot} given in figure 12.

Figures 9 and 10 show, respectively, the measured and calculated values of the reduced electric field, E/N, and the atomic oxygen fraction, O/N, as a function of the CO_2 fraction in the initial mixture for a discharge current of 20 mA and 40 mA and for two different pressures with N the density calculated from the ideal gas law with the pressure and gas temperature obtained from the fit of the FTIR measurements. Note that the data for 100% CO_2 is consistent with previously measured data in similar conditions [35] (see previous section).

Overall, the trend of the self-consistently calculated reduced electric field with the CO_2 initial fraction for different pressures agrees fairly well with the experimentally measured E/N. However, discrepancies are still present and further investigation is required to clarify why the absolute value of E/N seems overestimated for all conditions and the effect of changing the pressure seems underestimated in the model at 40 mA. Different possibilities for improvements of the model were already given in [11] and concern the rate coefficients of several reactions involving charged species, stepwise ionization processes involving vibrationally and electronically excited CO and CO_2 molecules, the charged-particle transport model and the ion transport data. Using the effective diffusion scheme for charged-species transport rather than classical ambipolar diffusion gave a better agreement between calculated and experimental E/N in [14]. However, this study was done in pure CO_2 were the low electronegativity observed did not invalidate the use of effective ambipolar diffusion which is not the case anymore in the CO_2–O_2 mixture.

The atomic oxygen fraction, O/N, (figure 10) also shows a good trend with the CO_2 fraction but remains too high for all conditions. This discrepancy could be reduced by using Polak's cross sections for the O_2 dissociation by electron impact [25] and it is discussed in section 4.5.

In figure 11 we present the CO_2 dissociation fraction defined as:

$$\alpha = \frac{n_{CO}}{n_{CO} + n_{CO_2}} \tag{16}$$

as a function of the gas mixture at different pressures and currents when the vibrational kinetics of CO_2 and CO are excluded or included in the model. No error bars are included in figure 11 for the CO_2 dissociation fraction, since in these conditions the reproducibility of the experimental results is very good, and the errors associated with the fitting of the FTIR spectra are smaller than the size of the symbols. For all the conditions, the CO_2 dissociation fraction decreases with increased O_2 content in the mixture and the main mechanisms contributing to this effect will be discussed in section 4.4. Moreover, the dissociation fraction α increases when the vibrational kinetics are considered. This can be a result of modifications of the EEDF or because of the contribution of the vibrationally excited states of CO_2 to the dissociation by

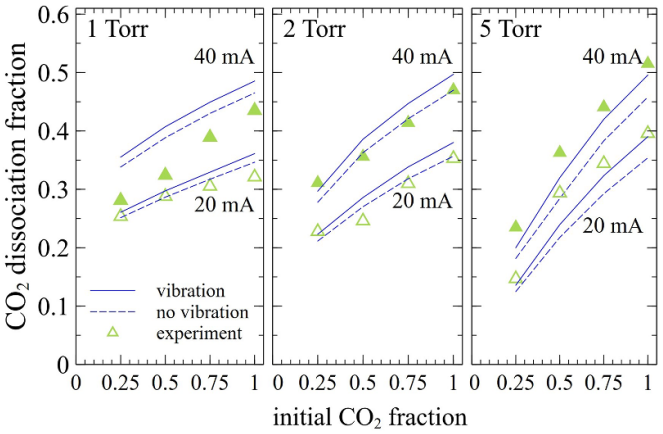

Figure 11. CO_2 dissociation fraction of a CO_2–O_2 discharge as a function of the CO_2 initial fraction in the CO_2–O_2 mixture at 20 mA and 40 mA: experiment (Δ), model calculations by excluding (– –) and including (—) the vibrational kinetics. No error bars are included in this figure, since the fitting error of the FTIR spectra and the reproducibility error of the experimental results are smaller than the size of the symbols.

electron impact. Indeed, the rate coefficients for the latter process are higher from the vibrationally excited states than from the ground state, due to the threshold shift in the dissociation cross sections for the vibrationally excited levels of CO_2. In addition, the high energy tail of the EEDF can be enhanced due to superelastic collisions with vibrationally excited CO and CO_2. The effect of the vibrational populations of CO and CO_2 in the electron kinetics on the EEDF was already thoroughly studied for pure CO_2 plasmas in [11, 14]. In particular, model calculations including and excluding the vibrational kinetics, and considering vibrational excited states only in the electron Boltzmann equation were done in [11] and the effect on the CO_2 dissociation fraction was shown in figure 4. Besides, the effect of considering the vibrational kinetics of CO_2 and CO in the Boltzmann solver on the EEDFs was studied in the modelling work of Silva *et al* [14]. The vibrational populations determine the rate of superelastic collisions with the vibrational levels and can therefore modify the high energy-tail of the EEDF increasing, by orders of magnitude, the electron impact excitation (including dissociation) and ionization rates [95–97]. In the system under study, CO_2 is essentially dissociated by direct electron impact, both on molecules in the vibrational ground-state ($00^00$1) and in vibrationally excited states. The contribution of the latter states comes mainly from the lower-laying levels ($01^10$1), ($02^20$1) and (10^002). At 1 Torr, and in pure CO_2, which corresponds to the condition of highest $T_{1,2}$ and T_3, 85% of the dissociation occurs from the ground state (GS). Moreover, for this case, the population of CO_2 in the GS is 0.67 and the corresponding dissociation rate coefficient from the (01^10) and the (02^20) levels is less than twice the rate coefficient from the GS. We thus conclude that, in our conditions, superelastic collisions have a prominent role on the enhancement of the CO_2 dissociation.

To investigate the effect of the discharge current on different plasma parameters, we performed simulations at 20 mA and 40 mA. The conversion is strongly correlated to the discharge current and the dissociation fraction, α, is increased by ∼0.11, both in the simulations and experiment when increasing the current from 20 mA to 40 mA (figure 11). Indeed, increasing the current changes the electron density in an almost linear way and in turn more electrons participate to the dissociation of CO_2.

At low pressure the experimental values are closer to the case without vibrations and always lower than the model. At 2 Torr, we can see that the agreement improves and finally at the highest pressure the experimental values are closer to the calculations performed with vibrations. This suggests that at higher pressure it is more important to take into account the vibrational kinetics to describe the chemistry in the discharge and at lower pressure the effect of the walls (both directly in the chemistry in surface reactions and in the vibrational kinetics) is not fully reproduced by the model.

Figure 12 shows the vibrational temperatures for CO and for the different modes of CO_2 obtained from the model and experiment as well as the rotational temperature T_{rot} used as input parameter for the model. They are in very good agreement and the discrepancy for T_{CO}, especially at 1 Torr comes from the signal to noise ratio worsening because of the lower density in general and because the dissociation is relatively low at 20 mA. For all the conditions under study, $T_{1,2}$ is almost in equilibrium with T_{rot} ($\sim T_g$) but T_{CO} is higher than T_3 which is higher than $T_{1,2}$. T_{CO} showing larger values than T_3 can be explained by different rate coefficients for V-T relaxation, the lack of inter-mode V-V relaxation processes affecting $CO_2(\nu_3)$ ($CO_2(\nu_3)+ CO_2(\nu_{1,2}) \rightarrow CO_2(\nu_3 - 1)+ CO_2(\nu_{1,2} + 1)$) but not CO, and more efficient vibrational excitation through electron-to-vibrational energy transfers for CO [35].

We can see in figure 12 that the temperatures T_3 and $T_{1,2}$ are slightly decreasing with increasing O_2 content. Indeed, the atomic oxygen density is higher when the O_2 content increases (figure 10) and therefore the quenching of the CO_2 vibrations by O atoms, which is an efficient process, is more important. We can also notice an opposite trend for the T_{CO}, that can be explained by the dependency of the rate coefficient for the CO_2–CO V-V transfer on T_g. Indeed, T_g decreases with the O_2 proportion, which leads to a smaller rate coefficient for this process. Moreover, the dilution of the CO_2 and CO molecules when O_2 is added can also explain the trend observed. The collisions and therefore vibrational energy transfer between CO and CO_2 are reduced because these molecules are diluted, and the CO_2 molecules will have more collisions with O_2 molecules with whom the vibrational energy transfer is much less efficient than with CO molecules. This effect contributes to reduce T_3 and $T_{1,2}$ and increase T_{CO} because of the reduced CO–CO_2 V-V (in addition to the effect of T_g). Note that the rate coefficient associated with the de-excitation of CO by O_2 is also increasing as a function of T_g but this increase is very slow in comparison with that of CO_2 and the absolute value is two orders of magnitude lower than for CO_2.

Finally, regarding the effect of pressure, we observe a smaller difference between the temperatures T_3 and T_{CO} (and T_3 and $T_{1,2}$) as pressure increases. This comes from the vibrational energy transfer from CO to ν_3 of CO_2, occurring due to its near resonant frequency, more effective at higher pressures

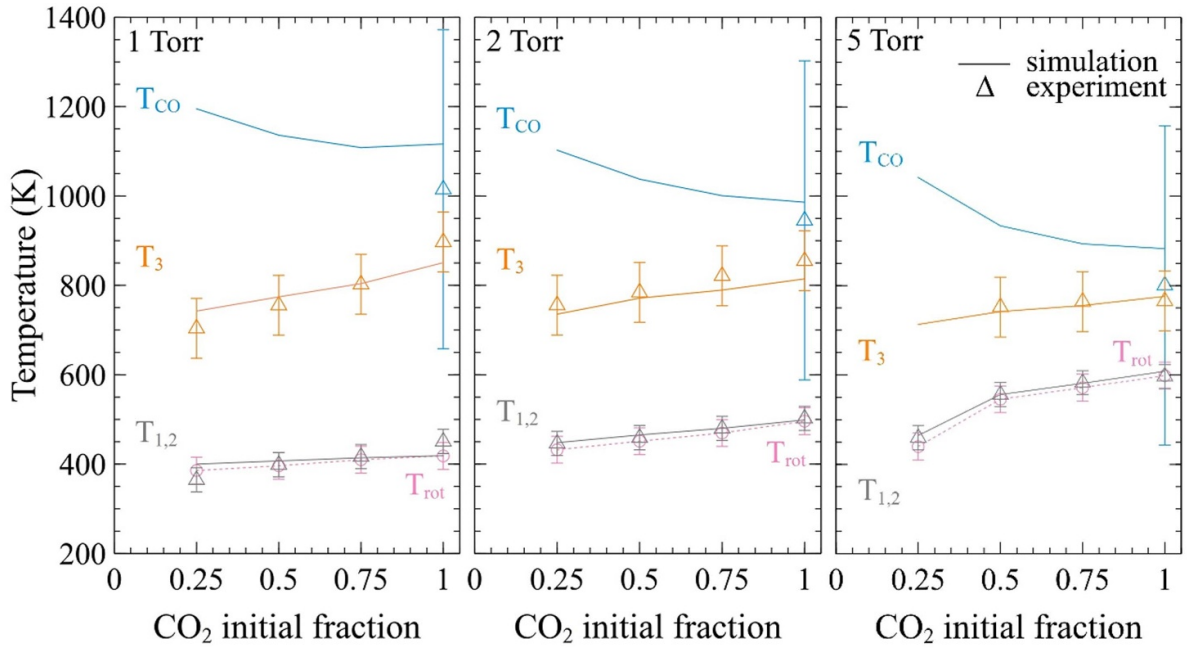

Figure 12. Experimental values (Δ) and calculated values (line) of the common vibrational temperature of the CO_2 bending and symmetric modes $T_{1,2}$, the vibrational temperature of the asymmetric stretching mode T_3, the CO vibrational temperature T_{CO} and the rotational temperature T_{rot} (used as input parameter for the model) when a discharge is ignited in different mixtures of CO_2–O_2, at current = 20 mA, and pressures of 1, 2 and 5 Torr. The error bars indicated were obtained in pure CO_2 at 5 Torr and 50 mA [26].

because of the higher collision frequencies. It was also verified that the change of $T_{1,2}$, T_3 and T_{CO} when increasing the current was well reproduced in the calculations.

4.4. Influence of the oxygen content on the CO_2 dissociation fraction

The admixture of O_2 has a detrimental impact on CO_2 decomposition since it leads to a decrease of the dissociation fraction defined as:

This effect was already observed experimentally by Grofulović *et al* [12] and confirmed in the present study (figure 11). Two main reasons were discussed briefly in the introduction, one of them being the enhancement of the reverse reaction producing back CO_2 in the presence of O_2 [13]. Another possible explanation was the quenching of vibrationally excited CO_2 by O atoms, but this option was discussed and discarded in section 4.2. One additional possible explanation could be the modification of the EEDF with increased oxygen content. As it can be seen in figure 13, the admixture of O_2 indeed modifies the EEDF, but it enhances the high energy tail which contributes to a higher dissociation fraction upon O_2 addition. Therefore, it cannot explain the observed behaviour.

The first aforementioned possible reason, the back-reaction mechanisms involving CO and O_2, requires further attention. There are several possibilities for these processes: reactions between ground-state molecules and reactions involving vibrationally or electronically excited CO. The experimental results and preliminary calculations by Morillo-Candas *et al* [13] and the kinetic modelling by Silva *et al* [32] show a key role of the metastable electronically excited state $CO(a^3\prod_r)$

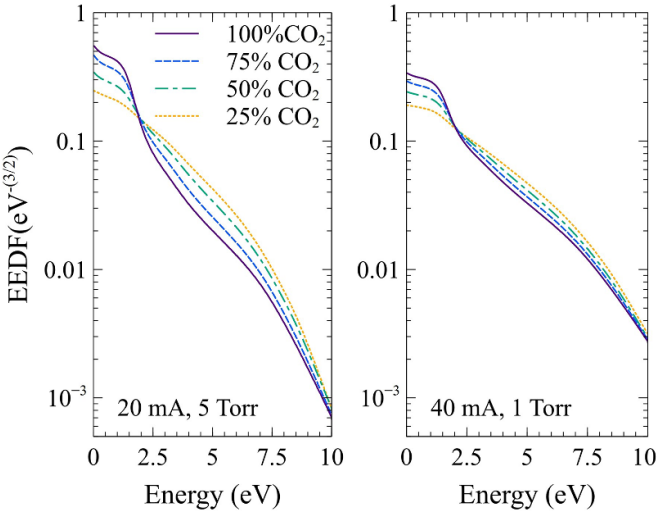

Figure 13. Electron Energy Distribution Functions calculated at $P = 5$ Torr and $I = 20$ mA (left panel), and $P = 1$ Torr and $I = 40$ mA (right panel), and input gas temperature from experiment, for different CO_2–O_2 mixtures, from 100% to 25% CO_2.

in the back-reactions, in low pressure pulsed glow and RF discharges. Indeed, the recombination of CO and O_2 both in the ground states producing CO_2 is a possible 'back reaction' but very slow at room temperature [98] and it is not even included in our model. This rate coefficient becomes significantly higher if the reaction involves vibrationally [26] or electronically excited CO molecules [13, 99]. Back-reactions based on the vibrationally excited CO were not dominant in

Table 5. Rate coefficients of the CO(a) quenching reactions used in this work, taken from [14].

Process	Rate coefficient in m^3s^{-1}
$CO(a) + O_2 \rightarrow CO + O_2$	2.4×10^{-17}
$CO(a) + O_2 \rightarrow CO + 2O$	2.4×10^{-17}
$CO(a) + O_2 \rightarrow CO_2 + O$	1.2×10^{-17}
$CO(a) + CO \rightarrow CO_2 + C$	9.1×10^{-19}
$CO(a) + CO \rightarrow 2CO$	5.6×10^{-17}
$CO(a) + CO_2 \rightarrow CO + CO_2$	5×10^{-18}
$CO(a) + CO_2 \rightarrow 2CO + O$	5×10^{-18}
$CO(a) + O \rightarrow CO + O$	1.9×10^{-16}

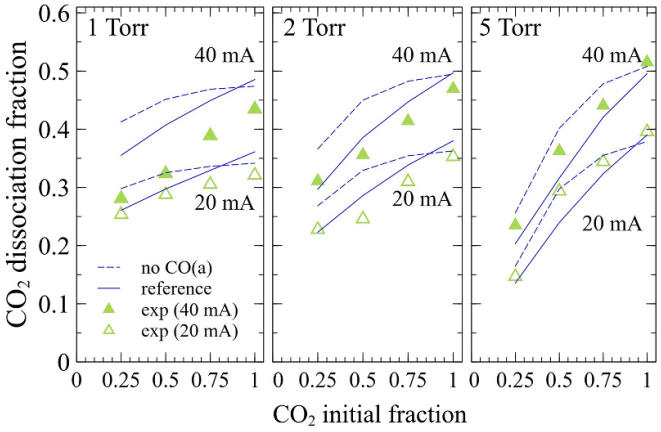

Figure 14. Experimental values (Δ, ▲) and calculated values (line) of the dissociation CO_2–O_2 mixtures, at 20 and 40 mA and 1, 2 and 5 Torr, including (—), same as in figure 11, and excluding (– –) the CO(a) state from the simulations.

their discharge conditions [13] but could become relevant at slightly higher vibrational temperatures, like in microwave discharges. Since the vibrational temperatures in those works are similar to the ones in our discharge, we can assume that vibrationally excited CO does not play an important role, in our conditions, for the back reactions.

The role of the electronically excited state $CO(a^3\prod_r)$, hereafter denoted CO(a), on CO_2 dissociation can be beneficial or detrimental for the CO_2 conversion. In fact, CO(a) can have an ambivalent role depending on the CO and O_2 density [100] as it either enhances the dissociation of CO_2 or stimulates the reconversion back to CO_2. Cenian *et al* [100] simulated glow discharges with similar working conditions to ours and brought up the ambivalent role of CO(a) and stressed its importance in the full description of CO_2 decomposition. Despite having a small molar fraction ($\sim 10^{-7}$), similar to what was reported in [14, 100], the energy of this state (~6 eV) is enough to dissociate CO_2 and O_2 molecules and, owing to this high energy, the rate coefficients of the processes involving CO(a) are close to the gas kinetic collision frequencies. The processes involving CO(a) and the corresponding rate coefficients are taken from Silva *et al* [14] and reported in table 5. This set of reactions gave a good agreement with experimental dissociation fraction of CO_2 in [14] and were in the range of possible values found in the literature. However, using different branching ratios can lead to good results as well. More details on the choice of these specific rate coefficients can be found in [14].

The lack of experimental data for branching ratios of the different dissociative quenching mechanisms of the CO(a) state has an impact on the simulated dissociation fraction, as pointed out in [14]. Furthermore, some energy transfer processes between vibrational CO(v) and CO(a), not included in the model, can take place in the system. For instance, the quenching of CO(a) via $CO(a) + CO \rightarrow 2CO(v)$ [84, 101] can produce vibrationally excited CO, while collisions between sufficiently energetic vibrational states can lead to CO(a) formation in $CO(v) + CO(w) \rightarrow CO(a) + CO$ [102]. Another possibly important process is the pumping of energy in the $v = 27$ level by quenching of CO(a), $CO(a) + CO \rightarrow CO(v = 27) + CO$ [84]. Finally, one can also consider the formation of the metastable through the following reaction $CO(v > 27) + CO \rightarrow CO(a) + CO$ [103]. These mechanisms were not included in this work as they are not likely to affect the results and conclusions in the steady-state conditions under study and would require an extended description of the CO vibrational kinetics. An assessment of the relevance of these energy transfer processes will be investigated in the future.

In order to assess the role of CO(a) in the present conditions, figure 14 compares the simulations where this state is included or excluded from the model. We can observe that, when CO(a) is added in the model, the dissociation fraction increases for CO_2 initial fraction of 0.75 and above, while below this turning point the dissociation fraction decreases. For gas mixtures with large amount of CO_2 but low CO density (low dissociation), the reaction $CO(a) + CO_2 \rightarrow 2CO + O$ contributes to enhance the dissociation. On the contrary, if the concentrations of CO and O_2 are larger the processes $CO(a) + O_2 \rightarrow CO_2 + O$ and $CO(a) + CO \rightarrow CO_2 + C$ are prevailing and lead to the CO_2 reconversion [13, 32, 100].

However, the presence of the CO(a) state alone does not explain entirely the increase of α with increased CO_2 concentration in the initial gas mixture. As can be seen on figure 14, even without including the CO(a) state in the chemistry the CO_2 dissociation fraction decreases with O_2 content in the discharge. Another process which could be responsible for the lower alpha when O_2 is added to the mixture is $O^- + CO \rightarrow CO_2$. To obtain more insight on the decrease of α with O_2 addition we studied the contribution to the main creation and destruction mechanisms of CO_2 molecules and how they evolve as a function of the initial CO_2 fraction. This is represented in figure 15.

The processes represented are, for the creation:

$$\begin{aligned} &C_1\text{: } CO(a) + O_2 \rightarrow CO_2 + O \\ &C_2\text{: } O^- + CO \rightarrow e + CO_2 \end{aligned} .$$

And for the destruction:

$$\begin{aligned} &D_1\text{: } e + CO_2 \rightarrow e + CO + O(^1D) \\ &D_2\text{: } CO(a) + CO_2 \rightarrow 2CO + O \end{aligned} .$$

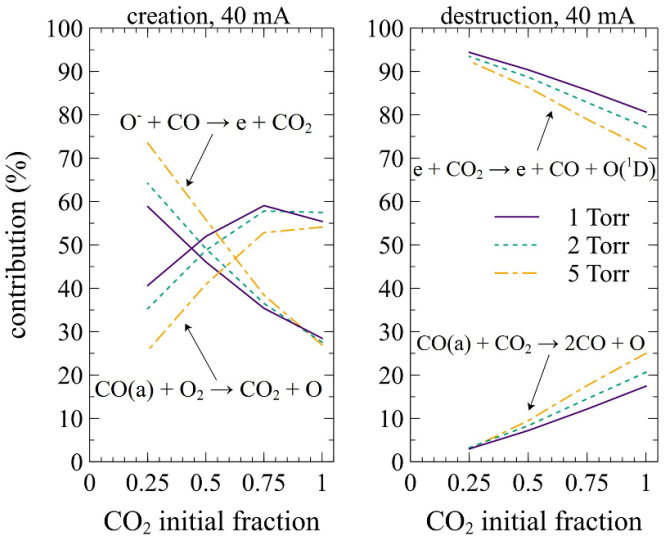

Figure 15. Contribution of the main creation (left) and destruction (right) processes for CO_2 at $P = 1$, 2 and 5 Torr and 40 mA for different CO_2–O_2 mixtures.

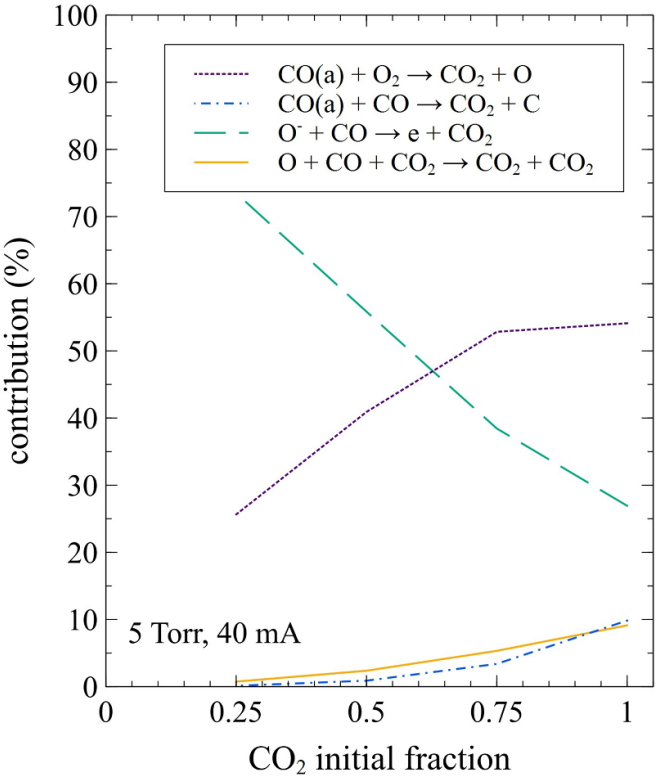

Figure 16. Contribution of the main creation processes for CO_2 at 5 Torr and 40 mA for different CO_2–O_2 mixtures.

The influence of the renewal of the gas due to the flow, which masks the importance of the other processes, is not considered in figure 15 (by removing its contribution and renormalized to 100% the contributions of all the other processes). The two main destruction mechanisms are then D_1 and D_2 and the two main creation mechanisms C_1 and C_2. The sum of contributions of D_1 and D_2 is always higher than 95% and a third minor contribution is coming from $e + CO_2 \rightarrow CO + O^-$. The sum of contributions of C_1 and C_2 is always higher than 94% except for the pure CO_2 case where two minor contributions coming from $CO(a) + CO \rightarrow CO_2 + C$ (for 1, 2 and 5 Torr) and $O + CO + CO_2 \rightarrow CO_2 + CO_2$ (only for 5 Torr) are important, as can be seen in figure 16. The addition of O_2 can also modify the ion conversion pathways and induce changes in the plasma parameters like the gas temperature [12].

4.5. O_2 dissociation cross sections

Two reactions account for O_2 dissociation by electron impact:

$$e + O_2 \rightarrow e + O(^3P) + O(^3P)\,(6eV) \qquad (17)$$

$$e + O_2 \rightarrow e + O(^3P) + O(^1D)\,(8.4eV) \qquad (18)$$

The dissociation through channel (15) occurs via the Herzberg states $O_2(A^3\Sigma_u^+, C^{3\Delta}_u, c^1\Sigma_u^-)$ and gives two oxygen atoms in the ground state. The oxygen dissociation corresponding to channel (16) occurs via the excitation of the $O_2(B^3\sum_u^+)$ state continuum and one of the oxygen atoms produced is in an electronically excited state $O(^1D)$. The continuum excitation of the $O_2(B^3\sum_u^+)$ state is usually the main contributor to the total cross-section of oxygen dissociation through electron impact. However, near the dissociation threshold the main contribution is made by the excitation of the Herzberg states with the energy threshold of around 6 eV. As indicated in the model description, our default cross sections for O_2 electron impact dissociation are taken from [46, 47]. However, it was reported that these cross sections may be overestimated and that it may be necessary to reduce the contribution from process (15) [104]. Thus, Kovalev *et al* used modified electron impact cross-sections for oxygen dissociation channels (15) and (16) as presented in [105] with respective thresholds of 5.58 and 7.34 eV. This modified cross-section set was verified by comparison with a large set of experimental data in different oxygen discharges [106, 107]. Other dissociation cross sections with lower amplitudes can be found in the literature. For instance, Polak and Slovetsky [25] computed the electron impact dissociation for cross-sections of O_2 and verified that the calculated cross-section of dissociation from the levels of the $O_2(B^3\sum_u^+)$ state was in satisfactory agreement with a few experimental points. Laporta *et al* [108] calculated a cross section for resonant electron impact dissociation of oxygen and Itikawa [109] reported a cross section for the total dissociation of O_2 in neutral products. The cross sections mentioned above are represented in figure 17.

In order to assess the influence of the O_2 electron impact dissociation cross section we make additional calculations by replacing the cross sections from Phelps [47] by the ones from Polak and Slovetsky [25]. However, similarly to what was done for the electron-impact dissociation of CO_2, we only use the cross sections from [25] to obtain the corresponding rate coefficient but not for the calculation of the EEDF.

In figure 18 we represent the dissociation fraction and the atomic oxygen fraction O/N, as well as the vibrational temperatures, $T_{1,2}$, T_3 and T_{CO}, for a discharge ignited in

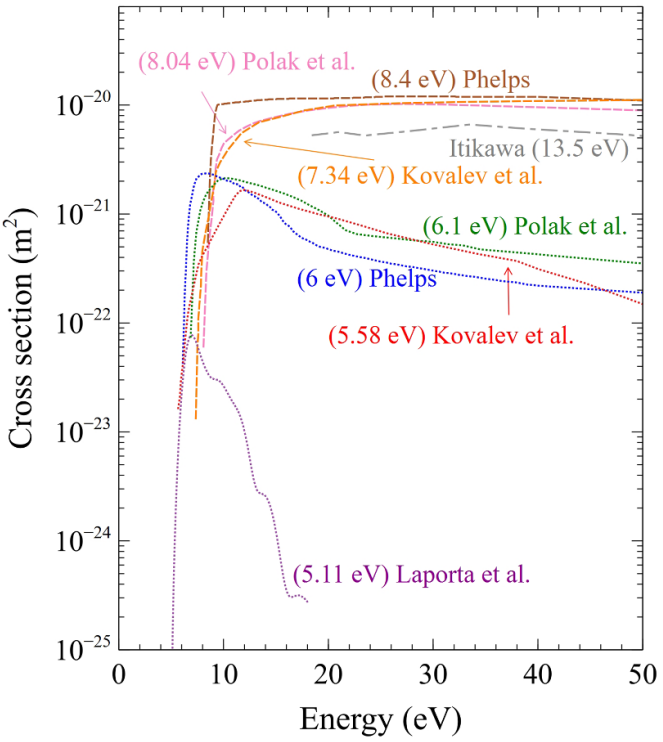

Figure 17. Dissociation cross sections of O_2, $e + O_2 \rightarrow O + O$ $(\cdots)$, $e + O_2 \rightarrow O + O(^1D)$ (– –), total dissociation (– - –) from different references mentioned in the text and the corresponding thresholds in parenthesis.

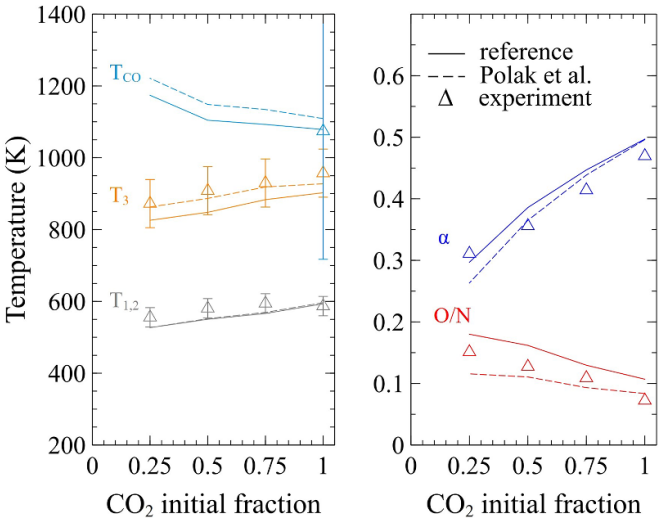

Figure 18. Experimental (Δ) and calculated values (line) of the common vibrational temperature of the CO_2 bending and symmetric modes $T_{1,2}$, the vibrational temperature of the asymmetric stretching mode T_3, the CO vibrational temperature T_{CO}, the dissociation fraction α and the atomic oxygen fraction O/N, for a discharge ignited in different CO_2–O_2 mixtures, at 40 mA and 2 Torr, using our reference cross section (—)[47]and the cross sections from Slovetsky *et al* [25] (– –) for O_2 dissociation.

different CO_2–O_2 mixtures, at 40 mA and 2 Torr. We can observe a decrease of the atomic oxygen fraction when using Polak's cross sections and a slight reduction of the dissociation fraction, more important at higher O_2 content. The vibrational temperatures, T_3 and $T_{CO,}$ are also impacted and increase for all conditions. Indeed, the main quenching mechanism for the CO_2 and CO vibrationally excited molecules occurs with atomic oxygen which becomes less important when O/N decreases. From this analysis we can conclude that using Polak's cross sections leads to a decrease of the calculated O/N but further work is necessary to understand the validity of this cross section.

4.6. Dominant mechanisms

The model developed in this work allows a further understanding of the complex coupled plasma kinetics, providing estimations of excited species densities, reaction rates or electron properties but also the relative contributions of the different processes to the formation and loss of the species considered. Being able to identify the processes ruling the discharge is essential to interpret experimental results as done in section 4.4. Figure 19 depicts the contributions of the dominant creation and destruction mechanisms of CO_2 and CO for two extreme conditions of pressure (1 and 5 Torr), for pure CO_2 and a 50/50 CO_2/O_2 mixture, at 20 mA. For each reaction we plot its relative importance for the creation (positive) or destruction (negative) of CO_2 (left panel) and CO (right panel).

To facilitate this study, the results are shown for simulations where the vibrational kinetics are not included.

In our conditions, the main CO_2 dissociation mechanism is by electron impact at ∼7 eV to create $O(^1D)$ and CO (R2), and ground-state CO molecules are essentially created by dissociation through electron impact on CO_2 molecules (R13). A dominant effect is the renewal of the gas (flow) controlling the loss of CO_2 and CO in this discharge (R2, R6, R9).

CO is also created from the quenching of the CO(a) state, mostly in collisions with CO and O, and to a lesser extend with CO_2 and O_2 (R12). CO(a) is obtained from the excitation of ground-state CO (via direct electron impact) which is one of the main processes of destruction of CO (R7). Therefore, reactions involving CO(a) and ground-state CO (R7, R11, R12) do not constitute true creation/destruction mechanisms of CO molecules, but only change the relative proportion of these two electronic levels. An effective creation mechanism of CO is the dissociation of CO_2 in collisions with CO(a), having a significant contribution to the production of CO. Finally, CO molecules are destroyed through the CO(a) state in the back reaction mechanism with O_2 giving back CO_2, $CO(a) + O_2 \rightarrow CO_2 + O$. It also corresponds to one of the main CO_2 creation channels (R5) contributing to more than 10% of CO_2 creation at 5 Torr, for the CO_2/O_2 mixture. Finally, CO_2 is mostly produced by renewal of the gas (R6).

As could be expected, the addition of O_2 to the CO_2 plasma changes the relative contributions of the different processes. For instance, the two processes leading to CO_2 recombination, involve O^- (R4) and O_2 (R5) species and gain importance when O_2 is added to the mixture, with respective contributions going from 4% to 22% and from 6% to 13%, at 5 Torr, whereas the contribution of the process leading to the dissociation of

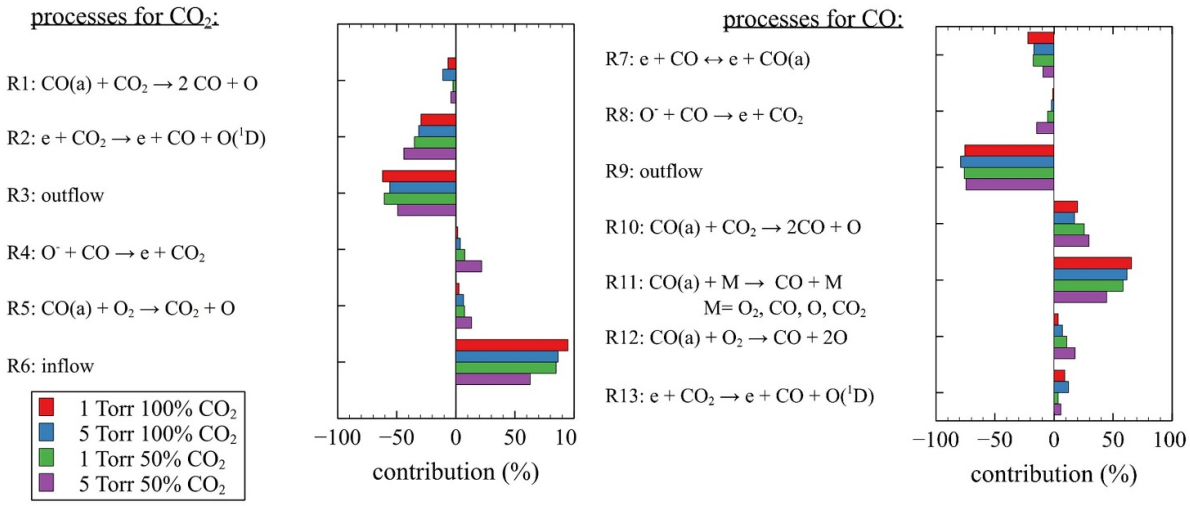

Figure 19. Contribution of different processes for creation (+)/ destruction (−) of CO_2 (left panel) and CO (right panel) for a low pressure (1 Torr) and for a high pressure (5 Torr) conditions, at 20 mA for pure CO_2 and a mixture of 50% CO_2 and 50% O_2.

CO_2 by collision with CO(a) (R1) is decreased upon O_2 addition. Finally, O^- ions influence the neutrals chemistry creating CO_2 back from CO in the recombination reaction (R4). The effect of the negative O ions on the neutrals chemistry was already observed in [14] but at a higher current (50 mA). Indeed, at low current, O^- is mostly created by dissociative attachment with CO_2 and mainly destroyed in the reverse reaction. However, at high current or in our case, when O_2 is added to the mixture, the production of O^- shifts towards dissociative attachment with O_2 and O^- then reacts with CO producing CO_2. This process can explain, at least partly, the detrimental effect of O_2 on the CO_2 dissociation as explained in section IV.4.

The differences between the two cases of different pressure are not significant but the creation of CO by electron impact (R13) is enhanced at higher pressure. Moreover, the quenching of CO(a) to CO (R11, R12) is more important at 1 Torr leading to a lower contribution of the CO(a) $+CO_2 \rightarrow 2CO + O$ reaction (R1). Indeed, the main quenching of CO(a) occurs with CO and O and while the CO fraction remains almost constant with pressure, O/N is much higher at 1 Torr than 5 Torr (figure 10).

5. Conclusion

This work presents a model that includes the state-to-state kinetics of the first 72 low-lying levels of CO_2 corresponding to the vibrational levels with ${v_1}^{max} = 2$ and ${v_2}^{max} = {v_3}^{max} = 5$ and energies up to about 2 eV and the 10 first levels of CO as well as the chemical kinetics of CO_2 and dissociation products. It constitutes a step forward towards a more complete and thorough validation of CO_2 dissociation in LTPs. Indeed, we extended the model from Ogloblina *et al* [11, 17–19], previously validated for low pressure DC glow discharge in a CO_2 plasma, by including the CO vibrational kinetics (e-V, V-V and V-T), the deactivation of CO_2 vibrationally exited molecules in collisions with O, CO and O_2, and also the CO2-CO V-V transfers, relevant in the context of CO_2 dissociation. For future studies, higher vibrational levels, up to the dissociation limit, should be included to better understand the underlying kinetics under a higher excitation regime. This should allow applying the model to plasma conditions targeted for CO_2 conversion on the industrial scale. This effort will involve the computation and validation of the rate coefficients involving highly vibrationally excited CO_2 molecules. However, first-order perturbation theories, like the SSH and SB approaches, while providing a good basis allowing for the description of CO_2 vibrations under low excitation regimes, cannot be used for the scaling of vibrational rates up to the dissociation limit. Different scaling procedures must be considered in future research.

The model was validated as a result of the good agreement between the calculated vibrational temperatures, O/N, E/N and dissociation fractions, and the corresponding experimental data measured in a DC glow discharge by *in situ* FTIR spectroscopy and actinometry. The reaction mechanism (validated set of reactions and corresponding rate coefficients) we propose predicts the quantities mentioned above for pressures between 0.4 and 5 Torr, discharge current of 20 and 40 mA and for different compositions ranging from 100% to only 25% of CO_2 in a CO_2–O_2 mixture.

The experimental trends associated with different pressures and mixtures were analysed. The experimental data show a lower conversion of CO_2 when O_2 is added to the plasma. The modelling study strongly suggests that this effect cannot be attributed to the quenching by O atoms of the vibrationally excited CO_2 but rather to enhanced back reactions involving the first electronically excited state of CO, CO(a), in combination with molecular oxygen or to a lesser extent with CO. Indeed, even though electronically excited states are often neglected in the study of plasma chemistry in CO_2 plasmas, they carry a significant amount of energy than can influence the heavy species chemistry under discharge conditions. When

the CO and O_2 densities become large enough, an important contribution of back reaction mechanisms controlled by electronically excited CO have been demonstrated and the role of $CO(a) + O_2 \rightarrow CO_2 + O$ is especially relevant for CO_2–O_2 mixtures. Finally, another process is also responsible for the lower alpha when O_2 is added to the mixture, $O^- + CO \rightarrow e + CO_2$, which becomes dominant for large O_2 fractions.

The similar thresholds for CO_2 dissociation through electron impact at ∼7 eV and back reaction mechanisms controlled by electronically excited states of CO at ∼6 eV suggest that effective separation of the dissociation products could enhance the CO_2 conversion efficiency. Future research should, therefore, concentrate on the development of separation procedure to isolate O_2 from the other dissociation products. Even though O atoms are not directly responsible for the reduced dissociation, their recombination at the wall to form O_2 is a key process [13, 31], and the use of membranes to extract O atoms from the plasma could thus enhance the conversion efficiency. Recent proposals for products separation include the use of silver membranes by Premathilake *et al* and Wu *et al* [110, 111], hollow fiber mixed-conductor membranes [112] and a new electrochemical membrane reactor presented by Goede [7].

The choice of cross sections as well as the values of recombination probability of O at the walls are very important parameters which determine the atomic oxygen density in the discharge. The choice of the appropriate electron impact cross section for O_2 dissociation remains an open question, but the present work brings further insight into it.

The present results confirm the non-equilibrium nature of low-pressure CO_2 plasmas, with a characteristic temperature of CO, T_{CO}, well above the temperature of the asymmetric vibration mode, T_3, which in turn is above the vibrational temperatures of the other two modes, $T_{1,2}$, and the gas temperature, T_g. Moreover, this study also corroborates the importance of the vibrational transfer from CO to the asymmetric stretching mode of CO_2, of the quenching of vibrationally excited CO_2 and CO by O atoms and subsequent reduction of the CO_2–CO V-V, in an accurate description of the vibrational kinetics in CO_2 plasmas. For the current discharge configuration, CO_2 dissociation is driven by electron impact and vibrational excitation plays a negligible role in both the dissociation via the ladder climbing mechanism and in the back reaction mechanisms, due to the low excitation regime in the glow discharge. Nevertheless, vibrational kinetics has a significant influence in dissociation via the electron superelastic collisions with vibrationally excited CO and CO_2 molecules modifying the EEDF and leading to an increase of the electron impact dissociation rate coefficients and, accordingly, of the CO_2 dissociation.

Data availability statement

The data that support the findings of this study are available upon reasonable request from the authors.

Acknowledgments

This work was partially supported by the European Union's Horizon 2020 research and innovation programme under Grant Agreement MSCA ITN 813393, and by Portuguese FCT-Fundacọ̃o para a Ciência e a Tecnologia, under Projects UIDB/50010/2020, UIDP/50010/2020, PTDC/FIS-PLA/1616/2021, EXPL/FIS-PLA/0076/2021 and PD/BD/150414/2019 (PD-F APPLAuSE). ASMC was funded by LabEx Plas@par receiving financial aid from the French National Research Agency (ANR) under project SYCAMORE, reference ANR-16-CE06-0005-01.

ORCID iDs

C Fromentin https://orcid.org/0000-0002-8230-2322
T Silva https://orcid.org/0000-0001-9046-958X
T C Dias https://orcid.org/0000-0002-2179-1345
A S Morillo-Candas https://orcid.org/0000-0002-6974-1240
O Biondo https://orcid.org/0000-0002-8061-4525
O Guaitella https://orcid.org/0000-0002-6509-6934
V Guerra https://orcid.org/0000-0002-6878-6850

References

[1] Allan R P, Hawkins E, Bellouin N and Collins B 2021 IPCC, 2021: summary for policymakers
[2] Lacis A A, Schmidt G A, Rind D and Ruedy R A 2010 Atmospheric CO_2 : principal control knob governing earth's temperature *Science* **330** 356–9
[3] Takht Ravanchi M and Sahebdelfar S 2021 Catalytic conversions of CO_2 to help mitigate climate change: recent process developments *Process Saf. Environ. Prot.* **145** 172–94
[4] Ashford B and Tu X 2017 Non-thermal plasma technology for the conversion of CO_2 *Curr. Opin. Green Sustain. Chem.* **3** 45–49
[5] Snoeckx R and Bogaerts A 2017 Plasma technology—a novel solution for CO_2 conversion? *Chem. Soc. Rev.* **46** 5805–63
[6] Kamkeng A D N, Wang M, Hu J, Du W and Qian F 2021 Transformation technologies for CO_2 utilisation: current status, challenges and future prospects *Chem. Eng. J.* **409** 128138
[7] Goede A P H 2018 CO_2 neutral fuels *EPJ Web Conf.* **189** 00010
[8] Bogaerts A and Neyts E C 2018 Plasma technology: an emerging technology for energy storage *ACS Energy Lett.* **3** 1013–27
[9] Ong M Y, Nomanbhay S, Kusumo F and Show P L 2022 Application of microwave plasma technology to convert carbon dioxide (CO_2) into high value products: a review *J. Clean. Prod.* **336** 130447
[10] Bogaerts A, Kozák T, van Laer K and Snoeckx R 2015 Plasma-based conversion of CO_2 : current status and future challenges *Faraday Discuss.* **183** 217–32
[11] Ogloblina P, Morillo-Candas A S, Silva A F, Silva T, Tejero-del-Caz A, Alves L L, Guaitella O and Guerra V 2021 Mars *in situ* oxygen and propellant production by non-equilibrium plasmas *Plasma Sources Sci. Technol.* **30** 065005

[12] Grofulović M, Klarenaar B L M, Guaitella O, Guerra V and Engeln R 2019 A rotational Raman study under non-thermal conditions in pulsed CO_2—N_2 and CO_2—O_2 glow discharges *Plasma Sources Sci. Technol.* **28** 045014

[13] Morillo-Candas A S, Guerra V and Guaitella O 2020 Time evolution of the dissociation fraction in rf CO_2 plasmas: impact and nature of back-reaction mechanisms *J. Phys. Chem.* C **124** 17459–75

[14] Silva A F, Morillo-Candás A S, Tejero-del-Caz A, Alves L L, Guaitella O and Guerra V 2020 A reaction mechanism for vibrationally-cold low-pressure CO_2 plasmas *Plasma Sources Sci. Technol.* **29** 125020

[15] Morillo-Candas A S, Silva T, Klarenaar B L M, Grofulović M, Guerra V and Guaitella O 2020 Electron impact dissociation of CO_2 *Plasma Sources Sci. Technol.* **29** 01LT01

[16] Klarenaar B L M, Engeln R, van den Bekerom D C M, van de Sanden M C M, Morillo-Candas A S and Guaitella O 2017 Time evolution of vibrational temperatures in a CO_2 glow discharge measured with infrared absorption spectroscopy *Plasma Sources Sci. Technol.* **26** 115008

[17] Silva T, Grofulović M, Klarenaar B L M, Morillo-Candas A S, Guaitella O, Engeln R, Pintassilgo C D and Guerra V 2018 Kinetic study of low-temperature CO_2 plasmas under non-equilibrium conditions. I. Relaxation of vibrational energy *Plasma Sources Sci. Technol.* **27** 015019

[18] Grofulović M, Silva T, Klarenaar B L M, Morillo-Candas A S, Guaitella O, Engeln R, Pintassilgo C D and Guerra V 2018 Kinetic study of CO_2 plasmas under non-equilibrium conditions. II. Input of vibrational energy *Plasma Sources Sci. Technol.* **27** 115009

[19] Silva T, Grofulović M, Terraz L, Pintassilgo C D and Guerra V 2018 Modelling the input and relaxation of vibrational energy in CO_2 plasmas *J. Phys. D: Appl. Phys.* **51** 464001

[20] Terraz L, Silva T, Morillo-Candas A, Guaitella O, Tejero-del-Caz A, Alves L L and Guerra V 2019 Influence of N_2 on the CO_2 vibrational distribution function and dissociation yield in non-equilibrium plasmas *J. Phys. D: Appl. Phys.* **53** 094002

[21] Silva T, Grofulović M, Terraz L, Pintassilgo C D and Guerra V 2020 Dynamics of gas heating in the afterglow of pulsed CO_2 and CO_2–N_2 glow discharges at low pressure *Plasma Chem. Plasma Process.* **40** 713–25

[22] Pietanza L D *et al* 2021 Advances in non-equilibrium CO_2 plasma kinetics: a theoretical and experimental review *Eur. Phys. J.* D **75** 237

[23] Hecimovic A, D'Isa F A, Carbone E and Fantz U 2022 Enhancement of CO_2 conversion in microwave plasmas using a nozzle in the effluent *J. CO_2 Util.* **57** 101870

[24] Hecimovic A, D'Isa F, Carbone E, Drenik A and Fantz U 2020 Quantitative gas composition analysis method for a wide pressure range up to atmospheric pressure—CO_2 plasma case study *Rev. Sci. Instrum.* **91** 113501

[25] Polak L S and Slovetsky D I 1976 Electron impact induced electronic excitation and molecular dissociation *Int. J. Radiat. Phys. Chem.* **8** 257–82

[26] Fridman A A 2012 *Plasma Chemistry* (Cambridge: Cambridge University Press)

[27] Armenise I and Kustova E 2018 Mechanisms of coupled vibrational relaxation and dissociation in carbon dioxide *J. Phys. Chem.* A **122** 5107–20

[28] Grofulović M, Alves L L and Guerra V 2016 Electron-neutral scattering cross sections for CO_2: a complete and consistent set and an assessment of dissociation *J. Phys. D: Appl. Phys.* **49** 395207

[29] Ogloblina P, Tejero-del-Caz A, Guerra V and Alves L L 2020 Electron impact cross sections for carbon monoxide and their importance in the electron kinetics of CO_2—CO mixtures *Plasma Sources Sci. Technol.* **29** 015002

[30] Guerra V, Silva T, Ogloblina P, Grofulović M, Terraz L, da Silva M L, Pintassilgo C D, Alves L L and Guaitella O 2017 The case for *in situ* resource utilisation for oxygen production on Mars by non-equilibrium plasmas *Plasma Sources Sci. Technol.* **26** 11LT01

[31] Guerra V, Silva T and Guaitella O 2018 Living on mars: how to produce oxygen and fuel to get home *Europhys. News* **49** 15–18

[32] Silva T, Morillo-Candas A S, Guaitella O and Guerra V 2021 Modeling the time evolution of the dissociation fraction in low-pressure CO_2 plasmas *J. CO_2 Util.* **53** 101719

[33] Meunier N, Laribi S, Dubois L, Thomas D and De Weireld G 2014 CO_2 capture in cement production and re-use: first step for the optimization of the overall process *Energy Proc.* **63** 6492–503

[34] Morillo-Candas A S, Klarenaar B L M, Amoedo C, Guerra V and Guaitella O 2021 Effect of oxygen atoms on the vibrational kinetics of CO_2 and CO revealed by the use of a large surface area material *J. Appl. Phys.* **54** 095208

[35] Morillo-Candas A S, Drag C, Booth J-P, Dias T C, Guerra V and Guaitella O 2019 Oxygen atom kinetics in CO_2 plasmas ignited in a DC glow discharge *Plasma Sources Sci. Technol.* **28** 075010

[36] Klarenaar B L M, Morillo-Candas A S, Grofulović M, van de Sanden M C M, Engeln R and Guaitella O 2019 Excitation and relaxation of the asymmetric stretch mode of CO_2 in a pulsed glow discharge *Plasma Sources Sci. Technol.* **28** 035011

[37] Tejero-del-Caz A, Guerra V, Gonçalves D, da Silva M L, Marques L, Pinhão N, Pintassilgo C D and Alves L L 2019 The LisbOn KInetics Boltzmann solver *Plasma Sources Sci. Technol.* **28** 043001

[38] Alves L L*et al* The LisbOn KInetics - LoKI 2022 *N- Plasmas Reactive: Modelling and Engineering (N-PRiME) server* (available at: https://nprime.tecnico.ulisboa.pt/loki/) (Accessed 31 October 2022)

[39] Chantry P J 1987 A simple formula for diffusion calculations involving wall reflection and low density *J. Appl. Phys.* **62** 1141–8

[40] Kutasi K, Guerra V and Sá P 2010 Theoretical insight into Ar–O_2 surface-wave microwave discharges *J. Phys. D: Appl. Phys.* **43** 175201

[41] Biondo O, Fromentin C, Silva T, Guerra V, van Rooij G and Bogaerts A 2022 Insights into the limitations to vibrational excitation of CO_2 : validation of a kinetic model with pulsed glow discharge experiments *Plasma Sources Sci. Technol.* **31** 074003

[42] Guerra V, Tejero-del-Caz A, Pintassilgo C D and Alves L L 2019 Modelling N_2–O_2 plasmas: volume and surface kinetics *Plasma Sources Sci. Technol.* **28** 073001

[43] Alves L L 2014 The IST-LISBON database on LXCat *J. Phys.: Conf. Ser.* **565** 012007

[44] Pancheshnyi S *et al* IST-Lisbon database n.d. *LXCat* (available at: www.lxcat.net)

[45] Gousset G, Ferreira C M, Pinheiro M, Sa P A, Touzeau M, Vialle M and Loureiro J 1991 Electron and heavy-particle kinetics in the low pressure oxygen positive column *J. Phys. D: Appl. Phys.* **24** 290

[46] Alves L L, Coche P, Ridenti M A and Guerra V 2016 Electron scattering cross sections for the modelling of oxygen-containing plasmas* *Eur. Phys. J.* D **70** 124

[47] Phelps A V 1968 Rotational and vibrational excitation of molecules by low-energy electrons *Rev. Mod. Phys.* **40** 399–410

[48] Annušová A, Marinov D, Booth J-P, Sirse N, da Silva M L, Lopez B and Guerra V 2018 Kinetics of highly vibrationally excited O_2(X) molecules in inductively-coupled oxygen plasmas *Plasma Sources Sci. Technol.* **27** 045006

[49] Marinov D, Guerra V, Guaitella O, Booth J-P and Rousseau A 2013 Ozone kinetics in low-pressure discharges: vibrationally excited ozone and molecule formation on surfaces *Plasma Sources Sci. Technol.* **22** 055018

[50] Koelman P, Heijkers S, Mousavi S T, Graef W, Mihailova D, Kozak T, Bogaerts A and van Dijk J 2017 A comprehensive chemical model for the splitting of CO_2 in non-equilibrium plasmas *Plasma Process. Polym.* **14** 1600155

[51] Morillo Candas A 2019 Investigation of fundamental mechanisms of CO_2 plasmas *Doctoral Thesis* Université Paris-Saclay (ComUE) (available at: www.theses.fr/2019SACLX091) (Accessed 22 October 2022)

[52] Marrone P V and Treanor C E 1963 Chemical relaxation with preferential dissociation from excited vibrational levels *Phys. Fluids* **6** 1215

[53] Nagnibeda E and Kustova E 2009 *Non-Equilibrium Reacting Gas Flows* (Berlin: Springer) (https://doi.org/10.1007/978-3-642-01390-4)

[54] Kustova E, Savelev A and Armenise I 2019 State-resolved dissociation and exchange reactions in CO_2 flows *J. Phys. Chem.* A **123** 10529–42

[55] Herzberg G 1945 *Molecular Spectra and Molecular Structure. II. Infrared and Raman Spectra of Polyatomic Molecules* (New York: D. Van Nostrand company, Inc)

[56] Chedin A 1979 The carbon dioxide molecule *J. Mol. Spectrosc.* **76** 430–91

[57] Courtoy C-P 1957 Spectres de vibration-rotation de molecules simples diatomiques ou polyatomiques avec long parcours d'absorption: XII. Le spectre DE $C^{12}O^{16}_2$ entre 3500 ET 8000 CM^{-1} ET Les constantes moleculaires de cette molecule *Can. J. Phys.* **35** 608–48

[58] Kozák T and Bogaerts A 2014 Splitting of CO_2 by vibrational excitation in non-equilibrium plasmas: a reaction kinetics model *Plasma Sources Sci. Technol.* **23** 045004

[59] Huber K P, Herzberg G, Gallagher J and Johnson R D III 2011 NIST chemistry webbook

[60] Laporta V, Tennyson J and Celiberto R 2016 Calculated low-energy electron-impact vibrational excitation cross sections for CO_2 molecule *Plasma Sources Sci. Technol.* **25** 06LT02

[61] Capitelli M, Ferreira C M, Gordiets B F and Osipov A I 2000 *Plasma Kinetics in Atmospheric Gases* (New York: Springer Science & Business Media)

[62] Laporta V, Cassidy C M, Tennyson J and Celiberto R 2012 Electron-impact resonant vibration excitation cross sections and rate coefficients for carbon monoxide *Plasma Sources Sci. Technol.* **21** 045005

[63] Black G, Wise H, Schechter S and Sharpless R L 1974 Measurements of vibrationally excited molecules by Raman scattering. II. Surface deactivation of vibrationally excited N_2 *J. Chem. Phys.* **60** 3526–36

[64] Grigorian G M and Cenian A 2013 Heterogeneous vibrational relaxation of carbon monoxide *Phys. Chem. Chem. Phys.* **15** 6215

[65] Yaney P P and Parish J W 1999 Studies of surface deactivation of vibrationally-excited homonuclear molecules in gaseous discharge media using coherent anti-Stokes Raman spectroscopy (CARS) (Dayton Univ OH)

[66] Marinov D, Lopatik D, Guaitella O, Hübner M, Ionikh Y, Röpcke J and Rousseau A 2012 Surface vibrational relaxation of N_2 studied by CO_2 titration with time-resolved quantum cascade laser absorption spectroscopy *J. Phys. D: Appl. Phys.* **45** 175201

[67] Grigoryan G M, Kochetov I V and Kurnosov A K 2010 Vibrational distributions of CO molecules in a dc discharge in the presence of molecular oxygen admixture *J. Phys. D: Appl. Phys.* **43** 085201

[68] Blauer J and Nickerson G 1974 A survey of vibrational relaxation rate data for processes importantto CO_2-N_2-H_2O infrared plume radiation *7th Fluid and Plasma Dynamics Conf.* (Palo Alto, CA: American Institute of Aeronautics and Astronautics) (https://doi.org/10.2514/6.1974-536)

[69] Schwartz R N, Slawsky Z I and Herzfeld K F 1952 Calculation of vibrational relaxation times in gases *J. Chem. Phys.* **20** 1591–9

[70] Sharma R D and Brau C A 1969 Energy transfer in near-resonant molecular collisions due to long-range forces with application to transfer of vibrational energy from ν3 mode of CO_2 to N_2 *J. Chem. Phys.* **50** 924–30

[71] Sharma R D and Welsh J A 2009 Vibrational energy transfer in O_2(v=2–8)–O_2(v=0) collisions *J. Chem. Phys.* **130** 194306

[72] Ashmore P G and Donovan R J 1977 *Gas Kinetics and Energy Transfer* LondonThe Chemical Society *Specialist Periodical Reports* **2**

[73] Kreutz T G, O'Neill J A and Flynn G W 1987 Diode laser absorption probe of vibration-vibration energy transfer in carbon dioxide *J. Phys. Chem.* **91** 5540–3

[74] Pack R T 1980 Analytic estimation of almost resonant molecular energy transfer due to multipolar potentials. VV processes involving CO_2 *J. Chem. Phys.* **72** 6140–52

[75] Kee R J *et al* CHEMKIN collection, release 3.6 (San Digeo, CA)

[76] López-Puertas M, Rodrigo R, Molina A and Taylor F W 1986 A non-LTE radiative transfer model for infrared bands in the middle atmosphere. I. Theoretical basis and application to CO_2 15 μm bands *J. Atmos. Terr. Phys.* **48** 729–48

[77] López-Puertas M and Taylor F W 2001 *Non-LTE Radiative Transfer in the Atmosphere* (River Edge, NJ: World Scientific)

[78] Buchwald M I and Wolga G J 1975 Vibrational relaxation of CO_2(001) by atoms *J. Chem. Phys.* **62** 2828–32

[79] Cramp J H W and Lambert J D 1973 Vibrational relaxation of CO_2(v3) by O atoms *Chem. Phys. Lett.* **22** 146–9

[80] Center R E 1973 Vibrational relaxation of CO_2 by O atoms *J. Chem. Phys.* **59** 3523–7

[81] Castle K J, Kleissas K M, Rhinehart J M, Hwang E S and Dodd J A 2006 Vibrational relaxation of CO_2(ν2) by atomic oxygen *J. Geophys. Res. Space Phys.* **111** 1

[82] Cacciatore M and Due Billing G 1981 Semiclassical calculation of VV and VT rate coeffecients in CO *Chem. Phys.* **58** 395–407

[83] Plönjes E, Palm P, Chernukho A P, Adamovich I V and William Rich J 2000 Time-resolved Fourier transform infrared spectroscopy of optically pumped carbon monoxide *Chem. Phys.* **256** 315–31

[84] Pietanza L D, Colonna G and Capitelli M 2017 Non-equilibrium plasma kinetics of reacting CO: an improved state to state approach *Plasma Sources Sci. Technol.* **26** 125007

[85] Witteman W J 2013 The CO_2 Laser (Springer)

[86] Ehrhardt H, Langhans L, Linder F and Taylor H S 1968 Resonance scattering of slow electrons from H_2 and CO angular distributions *Phys. Rev.* **173** 222–30

[87] Kustova E V, Nagnibeda E A and Armenise I 2014 Vibrational-chemical kinetics in mars entry problems *Open Plasma Phys. J.* **7** 76–87

[88] Achasov O and Ragosin D 1986 Rate constants of V-V exchange for CO_2- GDL *Preprint 16* (Minsk, Bielarus: Institute of Heat and Mass Transfer)
[89] Rosser W A, Sharma R D and Gerry E T 1971 Deactivation of vibrationally excited carbon dioxide (001) by collisions with carbon monoxide *J. Chem. Phys.* **54** 1196–205
[90] Starr D F and Hancock J K 1975 Vibrational energy transfer in CO_2—CO mixtures from 163 to 406 °K *J. Chem. Phys.* **63** 4730–4
[91] Treanor C E, Rich J W and Rehm R G 1968 Vibrational relaxation of anharmonic oscillators with exchange-dominated collisions *J. Chem. Phys.* **48** 1798–807
[92] Bass H E 1973 Vibrational relaxation in CO_2/O_2 mixtures *J. Chem. Phys.* **58** 4783–6
[93] TAYLOR R L and Bitterman S 1969 Survey of vibrational relaxation data for processes important in the CO_2-N_2 laser system *Rev. Mod. Phys.* **41** 26–47
[94] Joly V and Roblin A 1999 Vibrational relaxation of CO_2 (m, nl, p) in a CO_2-N_2 mixture. Part 1: survey of available data *Aerosp. Sci. Technol.* **3** 229–238.
[95] Pietanza L D, Colonna G, D'Ammando G, Laricchiuta A and Capitelli M 2016 Electron energy distribution functions and fractional power transfer in "cold" and excited CO_2 discharge and post discharge conditions *Phys. Plasmas* **23** 013515
[96] Pietanza L D, Colonna G, D'Ammando G, Laricchiuta A and Capitelli M 2016 Non equilibrium vibrational assisted dissociation and ionization mechanisms in cold CO_2 plasmas *Chem. Phys.* **468** 44–52
[97] Pietanza L D, Colonna G, D'Ammando G, Laricchiuta A and Capitelli M 2015 Vibrational excitation and dissociation mechanisms of CO_2 under non-equilibrium discharge and post-discharge conditions *Plasma Sources Sci. Technol.* **24** 042002
[98] Homann K H, Baulch D L, Drysdale D D, Duxbury J and Grant S 1977 Evaluated kinetic data for high temperature reactions, vol 3: homogeneous gas phase reactions of the O_2-O_3 systems, the CO-O_2- H_2 system, and of sulphur-containing species. Butterworths, London-Bost *Ber. Bunsenges. Phys. Chem.* **81** 704
[99] Wysong I J 2000 Measurement of quenching rates of CO($a^3\Pi$,v=0) using laser pump-and-probe technique *Chem. Phys. Lett.* **329** 42–46
[100] Cenian A, Chernukho A, Borodin V and Śliwiński G 1994 Modeling of plasma-chemical reactions in gas mixture of CO_2 lasers I. Gas decomposition in pure CO_2 glow discharge *Contrib. Plasma Phys.* **34** 25–37
[101] Slanger T G, Black G and Fournier J 1975 Electronic-to-vibrational energy transfer between molecules *J. Photochem.* **4** 329–39
[102] Gorse C, Cacciatore M and Capitelli M 1984 Kinetic processes in non-equilibrium carbon monoxide discharges. I. Vibrational kinetics and dissociation rates *Chem. Phys.* **85** 165–76
[103] Porshnev P I, Wallaart H L, Perrin M-Y and Martin J-P 1996 Modeling of optical pumping experiments in CO. I. Time-resolved experiments *Chem. Phys.* **213** 111–22
[104] Kovalev A S, Lopaev D V, Mankelevich Y A, Popov N A, Rakhimova T V, Poroykov A Y and Carroll D L 2005 Kinetics of in oxygen RF discharges *J. Phys. D: Appl. Phys.* **38** 2360–70
[105] Ivanov V V, Klopovskii K S, Lopaev D V, Rakhimov A T and Rakhimova T V 2000 Nonlocal nature of the electron energy spectrum in a glow discharge in pure O_2: i. Nonlocal character of the electron distribution function *Plasma Phys. Rep.* **26** 972–9
[106] Ivanov V V, Klopovskii K S, Lopaev D V, Rakhimov A T and Rakhimova T V 2000 Nonlocal nature of the electron energy spectrum in a glow-discharge in pure O_2: II. Actinometry of O(^{3}P) atoms in a plasma at low gas pressures *Plasma Phys. Rep.* **26** 980–90
[107] Ivanov V V, Klopovsky K S, Lopaev D V, Rakhimov A T and Rakhimova T V 1999 Experimental and theoretical investigation of oxygen glow discharge structure at low pressures *IEEE Trans. Plasma Sci.* **27** 1279–87
[108] Laporta V, Celiberto R and Tennyson J 2015 Dissociative electron attachment and electron-impact resonant dissociation of vibrationally excited O_2 molecules *Phys. Rev.* A **91** 012701
[109] Itikawa Y 2002 Cross Sections for Electron Collisions With Carbon Dioxide *J. Phys. Chem. Ref. Data* **31** 749–67
[110] Premathilake D, Outlaw R A, Quinlan R A and Byvik C E 2019 Oxygen generation by carbon dioxide glow discharge and separation by permeation through ultrathin silver membranes *Earth Space Sci.* **6** 557–64
[111] Wu D, Outlaw R A and Ash R L 1996 Extraction of oxygen from CO $_2$ using glow-discharge and permeation techniques *J. Vac. Sci. Technol.* A **14** 408–14
[112] Chen G, Buck F, Kistner I, Widenmeyer M, Schiestel T, Schulz A, Walker M and Weidenkaff A 2020 A novel plasma-assisted hollow fiber membrane concept for efficiently separating oxygen from CO in a CO_2 plasma *Chem. Eng. J.* **392** 123699